NTNU – Trondheim
Norwegian University of
Science and Technology

Rate based modelling of CO2 removal using alkanolamines

Xixi Liu

Natural Gas Technology
Submission date: February 2014
Supervisor: Even Solbraa, EPT
Co-supervisor: Eivind Johannessen, Statoil ASA

Norwegian University of Science and Technology
Department of Energy and Process Engineering

I declare that this is an independent work according to the exam regulations of the Norwegian University of Science and Technology

Trondheim

23 February 2014

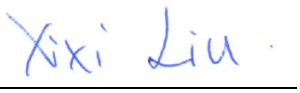

Xixi LIU

NTNU

Norwegian University
of Science and Technology

Department of Energy
and Process Engineering

EPT-M-2013-149

MASTER THESIS

for

student Xixi Liu

Autumn 2013

Rate based modelling of CO2 removal using alkanolamines
Ratebaserte modeller for CO2 fjerning med alkanolaminer

Background and objective
Components such as water, CO_2 and heavy hydrocarbons need to be removed from natural gas before it is cooled in a LNG process. These components can form solids during cool down if present at high concentrations and potentially block downstream process equipment.

Absorption in alkanolamines is a common method for removal of CO_2 from natural gas. For LNG production CO_2 needs to be removed to very low concentrations to prevent freezing in cryogenic process equipment. At Hammerfest LNG, CO_2 is removed from the natural gas to a concentration lower than 50 ppm (mole) using activated methydiethanolamine. Such a low concentration of CO2 in the LNG feed gas can only be obtained if the amine process is well designed and operated in an optimal and stable way.

The simulation and design of CO_2 removal processes using alkanolamines is challenging. Various methods have been developed for simulation of absorption and desorption of CO_2. Commercial process simulators will typically use either equilibrium- or a rate based model. The equilibrium based model is relatively simple where equilibrium CO_2 solubility is calculated and an approach to equilibrium is estimated. In the rate base model detailed mass transfer calculations between gas and liquid is done along the column.

The objective of this work will be to extend the mass transfer model developed during the student's project work. Both mass and heat transfer models in the liquid film will be studied during thesis work. Effect of CO_2-MEA equilibrium in liquid bulk should be considered.

The following tasks are to be considered:

1. Literature review of rate-based model of CO_2 absorption using alkanolamine solutions
2. Development of a film model with mass transfer of CO_2 into MEA by using Matlab
3. Evaluation of effect of temperature gradients in the film during CO_2 absorption
4. Development of a film model with mass and heat transfer during CO_2 absorption.

-- ” --

Within 14 days of receiving the written text on the master thesis, the candidate shall submit a research plan for his project to the department.

When the thesis is evaluated, emphasis is put on processing of the results, and that they are presented in tabular and/or graphic form in a clear manner, and that they are analyzed carefully.

The thesis should be formulated as a research report with summary both in English and Norwegian, conclusion, literature references, table of contents etc. During the preparation of the text, the candidate should make an effort to produce a well-structured and easily readable report. In order to ease the evaluation of the thesis, it is important that the cross-references are correct. In the making of the report, strong emphasis should be placed on both a thorough discussion of the results and an orderly presentation.

The candidate is requested to initiate and keep close contact with his/her academic supervisor(s) throughout the working period. The candidate must follow the rules and regulations of NTNU as well as passive directions given by the Department of Energy and Process Engineering.

Risk assessment of the candidate's work shall be carried out according to the department's procedures. The risk assessment must be documented and included as part of the final report. Events related to the candidate's work adversely affecting the health, safety or security, must be documented and included as part of the final report. If the documentation on risk assessment represents a large number of pages, the full version is to be submitted electronically to the supervisor and an excerpt is included in the report.

Pursuant to “Regulations concerning the supplementary provisions to the technology study program/Master of Science” at NTNU §20, the Department reserves the permission to utilize all the results and data for teaching and research purposes as well as in future publications.

The final report is to be submitted digitally in DAIM. An executive summary of the thesis including title, student’s name, supervisor's name, year, department name, and NTNU's logo and name, shall be submitted to the department as a separate pdf file. Based on an agreement with the supervisor, the final report and other material and documents may be given to the supervisor in digital format.

☐ Work to be done in lab (Water power lab, Fluids engineering lab, Thermal engineering lab)
☐ Field work

Department of Energy and Process Engineering, 04. September 2013

Olav Bolland

Department Head

Even Solbraa

Academic Supervisor

Eivind Johannessen (Statoil)
Research Advisors:

Acknowledgement

I am pleased to pay credit to **Department of Energy and Process Engineering in NTNU** for offering each possible facility and peaceful working environment in making my effort triumphant.

I would like to express my profound gratitude to my academic supervisor, **Professor Even Solbraa**, for his invaluable guidance and good advices throughout the challenging and exciting working period.

I would also like to thank my co-supervisor, **Eivind Johannesen** from Statoil, for his exceptional advices in the CO_2 capture field and for readily sharing his profound expertise in the most delightful manner.

Thanks a lot to my co-advisor, **Leila Faramarzi** from Statoil, for her unparalleled suggestions in Rate-based modeling field.

I would also like to thank **Zhicheng Xu**, a PhD student from Department of Thermal Engineering in Tsinghua University in China, for theoretically supporting on CO_2 chemical absorption. I would like to pay gratitude to PhD fellow **Rengarajan Soundararajan** for his support and helpfulness. His quest for preforming high quality research has inspired me and enabled me to complete this thesis work.

Finally, I am grateful to PhD fellows in Energy and Processing Department in NTNU for their helps and supports, and gratitude my friends and family for their love, encouragement during the whole work period.

Abstract

CO_2 is a major acid gas that is required to be removed from natural gas, in order to meet transportation specification. Chemical absorption using amine-based absorbents is a mature and well-known separation process applied on oil and gas industries. Due to the rate-controlled nature of reactive absorption process, classical steady-state equilibrium models are inadequate to describe the behavior and mechanical of chemical absorption processes. A more effective and accurate modelling approach is non-equilibrium model, which considers the thermodynamic driving forces across gas-liquid interface, and describes the actual rates of mass and heat transfer between gas and liquid phase.

In this thesis, a rate-based model for CO_2 chemical absorption by monoethanolamine (MEA) is developed. The rate-based model is presented based on two-film model that incorporates mass and heat transfer including CO_2-MEA chemical reactions. The model is implemented in MATLAB, and required parameters are determined by literature data.

This rate-based model consists of three parts: mass transfer model, temperature gradient estimation and heat transfer model. The first part of the model simulates the concentration profiles of CO_2 and MEA in the liquid film. This mass transfer model shows very good agreement with analytical literature results and with numerical simulation model developed during semester project.

In the second part of the model, the reaction heat and temperature gradient are estimated. Both of them decrease with distance from gas-liquid interface to liquid phase. This estimation model assumes that each grid in film segment is an adiabatic system. The maximum temperature gradient is approximately 6 K/s, and takes place at interface.

Heat transfer model, the third part of the model, estimates the temperature profile in the liquid film during CO_2 absorption by MEA. The temperature rise is due to physical absorption and exothermic chemical reaction. The temperature rise at interface simulated by heat transfer model is significantly lower than the rise-temperature simulated by temperature gradient model. This concludes that adiabatic assumption is not very realistic and heat conduction is necessarily considered in energy balance model. Furthermore, the heat transfer model shows that the temperature at interface is not raised significantly above the bulk temperature. Therefore, the effects of temperature rise on system physic-chemical properties, for instance to affect solubility, diffusivity and reaction rate, can be ignored.

This thesis investigates the effects of operation temperature, CO_2 loading and initial MEA mass weight on concentration profile, the distance of absorption equilibrium, temperature profile and temperature rise at the interface. The distance of absorption equilibrium preforms the opposite trend of temperature rise at interface.

In conclusion, this work addresses the development of a rate-based model for CO_2 absorption by MEA. The model predicted data is in accordance with published data.

Table of content

List of Figures

List of Tables

Nomenclature

Latin letter

A	Helmholtz Free Energy	J
C	Molar Concentration	kmol/m^3
c_p	Heat Capacity at Constant Pressure	kJ/(kg·K)
d	Hydraulic Diameter of the Column	m
D	Effective/Ficks Diffusion Coefficient	m^2/s
E	Murphree efficiency	-
E	Energy Flux	J/(m^2·s)
E	Enhancement Factor	-
f	Fugacity	bar
G	Gibbs Free Energy	J
h	Heat Transfer Coefficient	J/(m^2·s)
h	Height of the Column	m
H	Enthalpy	J
H	Henry's Law Constant	Pa·m^3/kmol
Ha	Hatta Number	-
k	Reaction Rate Constant	m^3/(kmol·s)
k_g	Mass Transfer Coefficient in Gas Phase	mol/(Pa·cm^2·s)
$k_G{}'$	Mass Transfer Coefficient in Liquid Phase	mol/(Pa·cm^2·s)
k_{obs}	Observed Reaction Rate Constant	1/s
k_{app}	Apparent Reaction Rate Constant	1/s
K_{eq}	Chemical Equilibrium Constant	-
K_G	Total Mass Transfer Coefficient	mol/(Pa·cm^2·s)
m	Molality	kmol/m^3
m	Mass	kg
M	Molecular Weight	kg/kmol
n	Mole Number	mol
N	Mass Transfer Flux	mol/(m^2·s)
Nu	Nesselt Number	-
P	Pressure	Pa
P	Products	
Pr	Prandtl Number	-
Q	Reaction Heat	J
r	Reaction Rate	kmol/(m^3·s)
R	Universal Gas Constant	J/kmol
R	Reactant	
Re	Reynolds Number	-
S	Entropy	J/K
Sc	Schmidt Number	-
Sh	Sherwood Number	-
T	Temperature	K
U	Internal Energy	J

V	Volume	m^3
x	Liquid Mole Fraction	-
y	Gas Mole Fraction	-
z	Axial coordinate	m
Δz	Segment thickness in liquid film	m

Greek Letter

α	Heat Conductive Coefficient	$W/(m^2 \cdot s)$
γ	Activity Coefficient	-
δ	Thickness of Gas/Liquid film	m
λ	Thermal Conductivity	$kW/m \cdot K$
ϑ	Stoichiom Etric Coefficient	-
μ	Viscosity	cP
μ	Chemical Potential	J/mol
ρ	Density	kg/m^3
φ	Fugacity Coefficient	-

Subscripts

b	Bulk
E	Entering Stream
i,j,k	Index
i	Interface
g	Gas
l	Liquid
L	Leaving stream
V	Vapor

Superscripts

*	Equilibrium state

1. Introduction

The removal of acid gas is an important industrial process, which has to be launched among the entire oil and gas processing. Acid gases, majority including carbon dioxide (CO_2), hydrogen sulphide (H_2S) and other sulphur species, have to be removed from natural gas before it is transported as sale gas to the customers. This is to meet transportation specification, and to maintain additional processing without corrosion or plugging problems. The H_2S concentration must be purified down to 6 mg/Nm^3, and the CO_2 concentration must be reduced down to 3-4 mol% (Engineering Data Book 2004). If the gas is being transported as LNG or fed to nitrogen rejection facility, the CO_2 concentration must be reduced less than 50 ppm, in order to avoid solid CO_2 formation during liquefying (Klinkenbijl 1999).

Acid gas removal technologies include absorption, adsorption, cryogenics and membranes. Novel variations of these technologies like solid sorbents, metal organic frameworks, enzyme-based system and ionic liquids have been developed for acid gas removal (Figueroa, Fout et al. 2008). Acid gas removal with aqueous amines is a mature technology that was first patented in 1930, and chemical absorption with amines has been practiced in the oil and gas industries for many years (Kohl 1997). Many solvents, such as Monoethanolamine (MEA), diethanolamine (DEA), methyldiethanolamine (MEAD) and piperazine (PZ) have been applied until now (Zhicheng Xu, Shujuan Wang et al. 2013). MEA has been employed as an important industrial absorbent due to its high reaction rate, relatively low cost and thermal stability(Campbell 1992).

Various models have been developed for simulation of reactive absorption and desorption of acid gases, since successful industrial applications were introduced in the 1980s (Peng, Lextrait et al. 2002). Commercial process simulators typically use either equilibrium model or non-equilibrium model. The equilibrium model is relatively simple where vapor-liquid equilibrium is assumed to take place at each stage. To adjust the equilibrium theoretical description to real conditions, tray efficiencies or height equivalent to a theoretical plate (HETP) are introduced (Baur, Higler et al. 2000, Taylor, Krishna et al. 2003). The non-equilibrium model assumes that the vapor-liquid equilibrium only occurs at the interface, and describes the mass transfer between gas and liquid (Peng, Lextrait et al. 2002, Asprion 2006).

This thesis is an extension of the project work. The major objective of the thesis is to develop a two-film model with mass and heat transfer during CO_2 absorption by using MEA. In summary, the four objectives are listed as follow:

1. Literature review of rate-based model of CO_2 absorption with aqueous alkanolamine solutions;
2. Comparison of two-film mass transfer model developed during thesis and project work;
3. Evaluation of the effect of temperature gradients in liquid film during CO_2 absorption;
4. Development of a two-film model with mass and heat transfer.

As a guide to the reader, the overall structure of thesis is presented here. In chapter 1, a brief introduction to the work and the objectives of the thesis are presented. Chapter 2 gives an overview of natural gas processing and acid gas removal technologies. In chapter 3, literature review of modelling of CO_2 absorption with aqueous alkanolamine solutions is described. This includes the comparison of equilibrium and non-equilibrium model applied in industrial simulations, chemical reaction kinetics mechanisms, and the mass and energy transfer relations. Chapter 4 describes the computational mass and heat transfer models in liquid film, which are implemented among the entire thesis work, and presents the required parameters. In chapter 5, the results of mass and heat transfer model are presented. The sensitivity analysis are discussed in chapter 6, including the effects of operation temperature, CO_2 loading and MEA mass weight on concentration profile, temperature profile in liquid film, absorption equilibrium thickness and temperature-rise at interface. Chapter 7 outlines the conclusion for the thesis and recommendation for the future work. In appendix, MATLAB codes are attached and simulation results are tabulated.

2. Backgrounds

2.1 Natural Gas Processing

Natural gas processing is an industrial process designed to clean raw natural gas by separating unwanted components, for example water, inert gases, acid gases and trace metals, to produce gas that meets transportation and commercial specifications. A typical natural gas processing chain on Norwegian Continental Shelf (NCS) is demonstrated in Figure 2-1, consisting separation, transportation and distribution. The important operations among natural gas chains have been systematically described by Rojey (Rojey 1997).

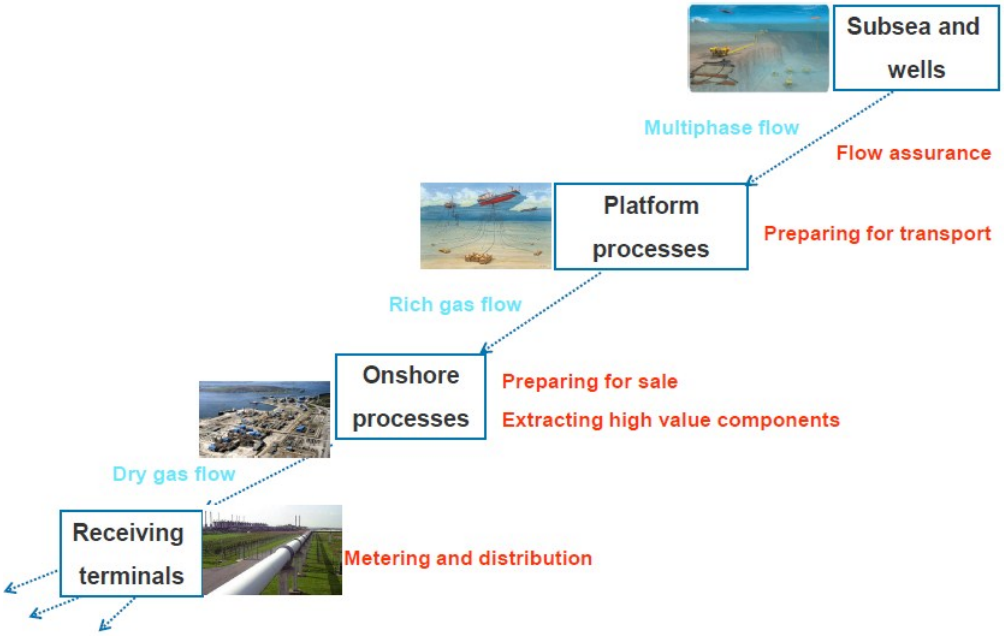

Figure 2-1 Typical gas processing value chain in Norwegian Continental Shelf

Firstly, natural gas is collected on the processing platform from reservoir and several wells by multiphase pipelines or subsea production system. The main purpose on the platform is to prepare natural gas in single-phase rich gas transport to shore where the gas is further processed to sales gas. The processing on the platform depends on the transportation form in associated with several factors, for example the distance to shore, the existing infrastructures and equipment. Nature gas can be transported from offshore to onshore via either pipelines or liquefied natural gas (LNG).

To ensure safety of natural gas transportation under corresponding transport conditions and commercial consideration, the specifications of procedures are needed to be met. The components required to be removed and the relevant reasons are listed as follow:

- Hydrogen sulphide (H_2S), toxic and corrosive
- Carbon dioxide (CO_2), corrosive, no heating value, crystallization in cryogenic process
- Trace metals, like mercury (Hg), toxic and corrosive in aluminum equipment
- Water, hydrate formation and corrosion
- Heavy hydrocarbons, condensing in transport systems
- Nitrogen (N_2), no heating valve

2.2 Acid Gas in Natural Gas

Acid gases, majority including carbon dioxide (CO_2), hydrogen sulphide (H_2S) and other sulphur species, need to be removed down to sufficiently low levels to meet transportation specification and to maintain additional processing without corrosion or plugging problems. The amount of acid gases in natural gas in the global field has been illustrated in Figure 2-2. H_2S is highly toxic, and forms a weak corrosive acid in the presence of water, whereas CO_2 is non-flammable and consequently undesirable in a fuel. It forms a weak corrosive acid in the presence of water. Although the toxicity of CO_2 is less than H_2S, it is heavier than air and can cause asphyxiation resulting in death in non-adequate ventilation system.

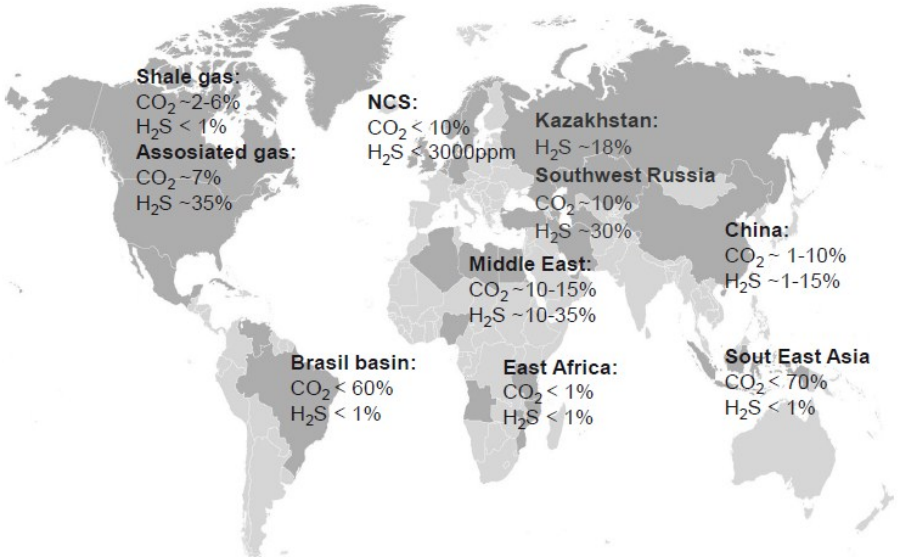

Figure 2-2 Acid gases amount in natural gas

Considering the problems of acid gases and the specification of acid gases during natural gas transportation, acid gas removal process has to be launched among the entire natural gas processing. Figure 2-3 demonstrates the block diagram of entire natural gas processing and highlights acid gas removal steps in red rectangles.

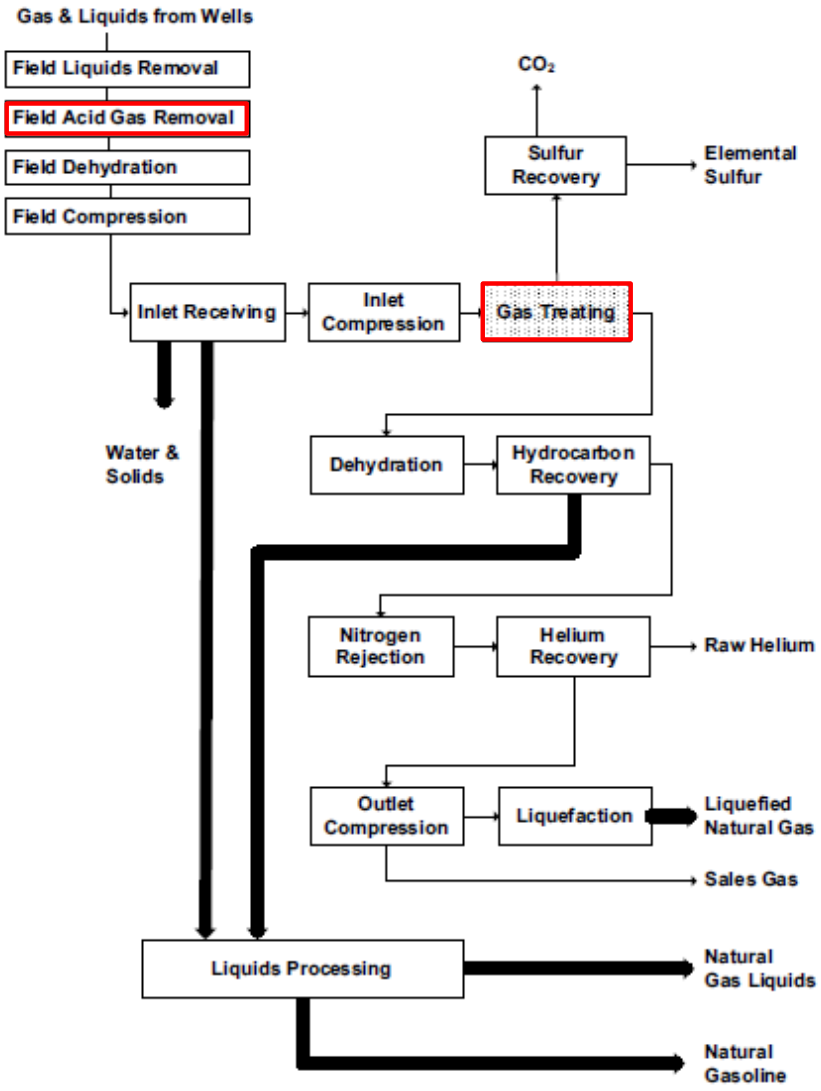

Figure 2-3 Block schematic of natural gas processing (Kidnay 2011), and red rectangles highlight the location of acid gas removal.

The specifications of processed natural gas need to be met considering the transport conditions or downstream utilization purposes (residential or industrial fuel). The H_2S concentration must be purified down to 6 mg/Nm^3, and the CO_2 concentration must be reduced down to 3-4 mol% (Engineering Data Book 2004). For example, CO_2 distributed to the European market from the Sleipner field in the North Sea is reduced to approximately 2.5 mol% to the next processing unit. On the other hand, if the gas is being

transported as liquefied natural gas (LNG) or fed to nitrogen rejection facility, the CO_2 concentration must be reduced less than 50 ppm, in order to avoid solid CO_2 formation during liquefying (Klinkenbijl 1999).

2.3 Acid Gas Removal Technology

Since the concentration of acid gases in raw gas and the acceptable levels in final product vary substantially due to for example geographical distribution of the raw gas, many removal processes have been currently applied. The acid gas removal processes generally include absorption, adsorption, cryogenics, membranes and microbial/algal system (Figure 2-4). Absorption includes chemical and physical processes. Chemical processes involve components of the solvent reacting with the acid gases while physical processes absorb the acid gases. Absorption using alkanolamines is a common industrial method to remove acid gases from natural gas (Figure 2-5). CO_2 removal process is more complex compared with other acid gas components, therefore CO_2 absorption using alkanolamines has been emphatically presented in this thesis work.

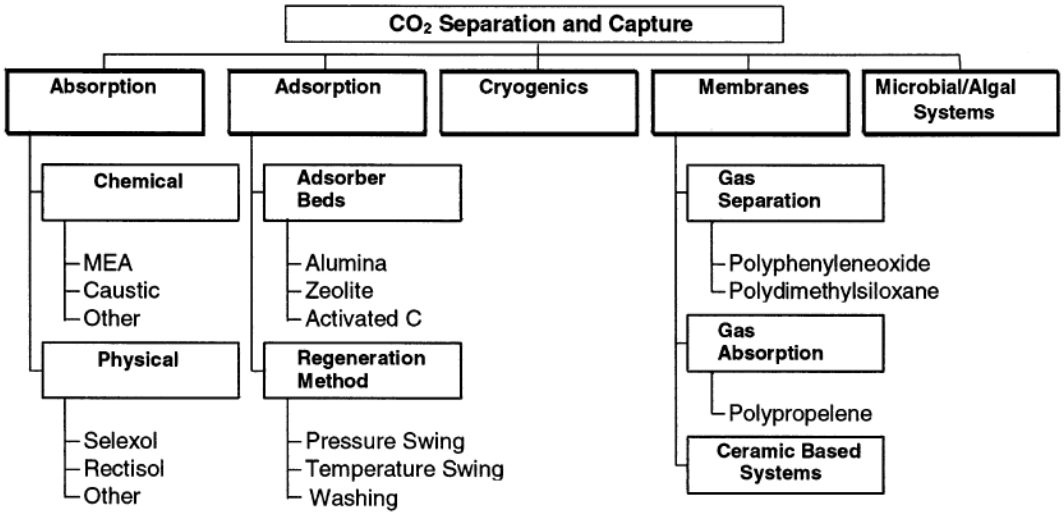

Figure 2-4 The common technology for acid gas separation and capture (Rao 2002).

The selection of acid gas removal processes also depends on other items, which are presented as follow:

- Type and concentration of impurities and hydrocarbon composition of the sour gas.
- Temperature at which the sour gas is processed.
- Partial pressure of acid gas in inlet and outlet of processing units.

- Specification of the outlet gas, the acid gas, and liquid products.
- Volume of gas.
- Desired selectivity for acid gas removal.
- Economics
- Environmental impacts, like air emission, waste water discharge, and disposal of by-products considered hazardous chemicals.

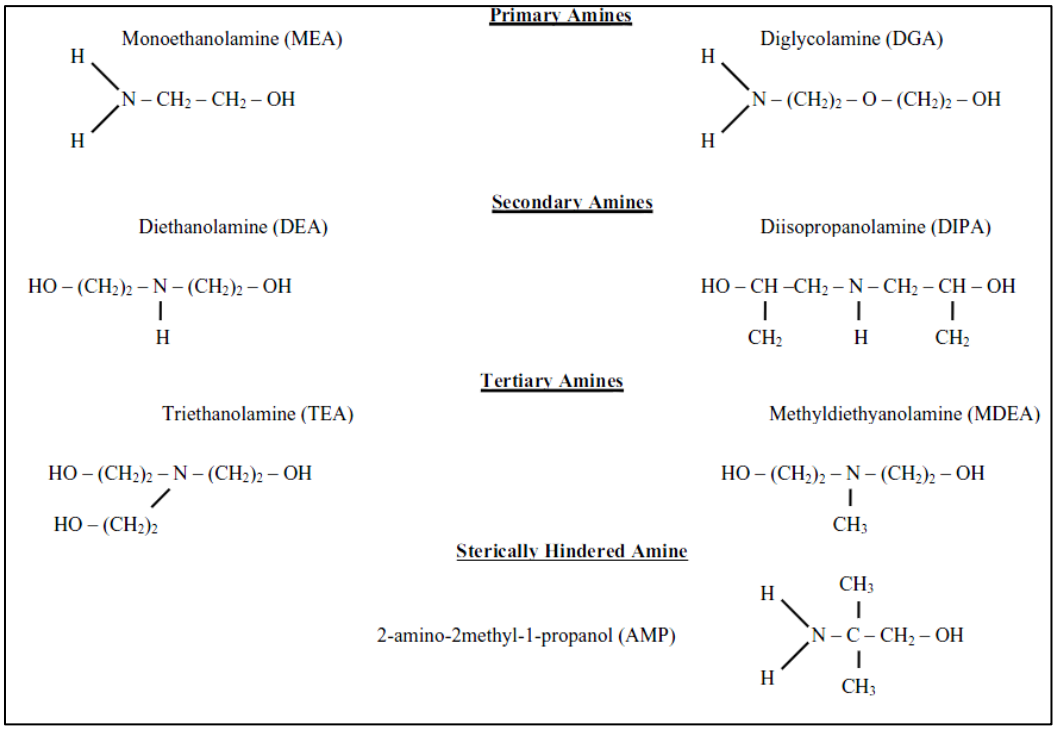

Figure 2-5 Molecular structures of commonly used amines in gas processing (Kidnay 2011).

The selection of CO_2 removal technologies is demonstrated in Figure 2-6 which shows the application range. The light blue areas represent the range of absorption processes, whereas the dark blue areas show the removal technologies based on adsorption and membrane. As shown in the figure, absorption processes are clearly the leading technology since they have been commercially deployed.

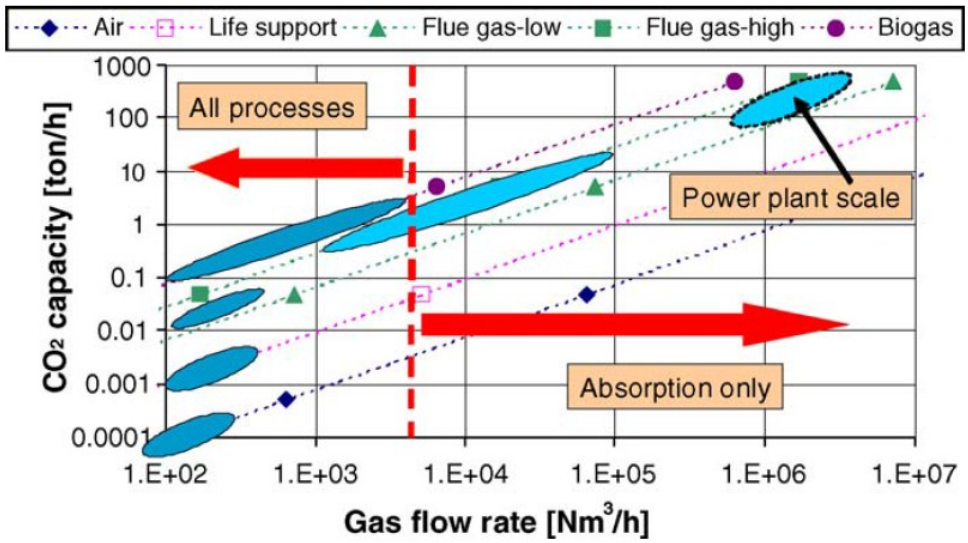

Figure 2-6 Application range for different technologies for CO_2 removal (Feron 2010)

2.3.1 Physical absorption

The basic principle of physical absorption is that the component being absorbed is more soluble in the liquid solvent than other component of the gas stream, and without chemical reaction with absorbent. The equilibrium concentration of the absorbate in the liquid solvent and the separation efficiency of mixed gas stream strongly depend on the partial pressure in the gas phase and physical differences between the components.

2.3.2 Chemical absorption

Chemical absorption is a two-step process for gas purification. Step one: physical absorption of a gas into the solvent; step two: reaction between the gas and the solvent. In acid gas removal process, the second step can be specified as that a weak acid formed by dissolved gas reacts with the weakly basic amine. Chemical reaction between the specific components in the gas stream and solvent is the key point where the components can be significantly reduced to meet the specification level.

Chemical reaction can be divided into two groups, irreversible and reversible reaction. The most common chemical absorption processes in gas processing, especially in acid gas removal process, is reversible reaction. That is why solvent regeneration process is installed after acid gas purification unit. The operation temperature and pressure in absorption and regeneration is corresponding to the chemical reactions.

2.4 Acid Gas Removal Process

This thesis work studies the modeling of CO_2 absorption using aqueous alkanolamine solutions, the acid gas chemical absorption process is presented here.

The simplified process of acid gas removal from natural gas with alkanolamines is demonstrated in Figure 2-7. The sour gas feed enters the bottom of the contractor at about 70 bar pressure and 30 °C temperature. The sour gas flows upward in the contactor, then countercurrent to the lean amine solution where flows downward. The lean amine that flows from the top of contactor is maintained at condition where the temperature is above the inlet gas, in order to prevent condensation of heavier hydrocarbon liquid formation.

The contactor operates above ambient temperature because the absorption between acid gas and alkanolamines is exothermic reaction. The maximum temperature is generally in the lower portion of the tower, which can be up to about 80 °C. The sweet gas (treated gas) leaves at the top of contactor where the temperature is around 38 °C controlled by the temperature of lean amine that enters.

The temperature of rich amine leaving the contactor bottom is around 60 °C. The pressure of rich amine is then decreased to 5-7 bar in a flash tank to remove dissolved hydrocarbon.

The rich amine enters the solvent regenerator at temperature in the range of 80 - 100 °C after passing through a heat exchanger. The vapor steams, which consist of acid gases and water vapor, generated from amine flows upward to further steps. The lean amine is removed from the regenerator and reenters at the top of the contactor to cycle the acid gas removal process.

CO_2 chemical absorption technology offers a range of advantages than other technologies. It is a mature technology that was first patented in 1930, and chemical absorption with amines has been practiced in the oil and gas industries for many years (Kohl 1997). Many solvents, such as Monoethanolamine (MEA), diethanolamine (DEA), methyldiethanolamine (MEAD) and piperazine (PZ) have been applied until now (Zhicheng Xu, Shujuan Wang et al. 2013). CO_2 recovery rates of 98% and product purity of 99% can be achieved by applying chemical absorption technology. The solvent can be regenerate since the reactions are reversible (*http:// CO2captureproject.org*).

The byproducts from reaction between CO_2 and amine, for instance carbonate or bicarbonate salts, require significant energy to regenerate in the stripper. Regeneration may enlarge 10-20% of the investment cost (Astarita 1983) The current amine

technologies may reduce up to 30 % power output and 10 % efficiency of power plants (EPRI 2012). Circulation rate affects the reboiler energy requirement, and increase 50-70% overall investment (Astarita 1983).

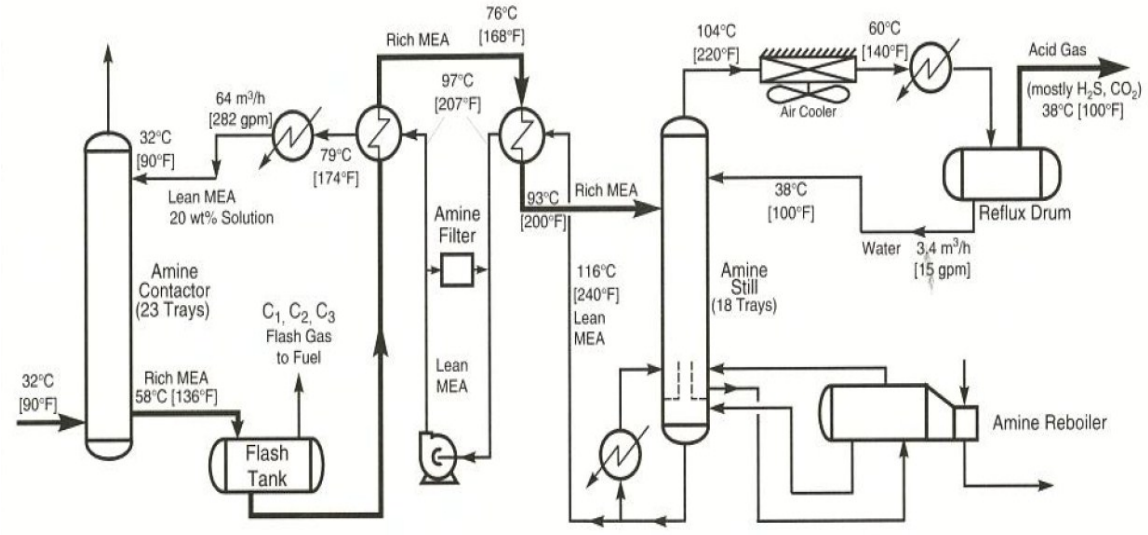

Figure 2-7 Process flow diagram for acid gas removal using amine solvent (Campbell 1992)

3. Literature Review of Modeling of CO_2 Absorption with Aqueous Alkanolamines Solutions

3.1 Equilibrium and Non-Equilibrium Model

For modelling reactive distillation columns, two different approaches are available in the literature. One is the equilibrium stage model, in which the vapor and liquid phase are assumed to be in the thermodynamic equilibrium. Another is the non-equilibrium stage model, in which the finite mass transfer rate across the vapor-liquid interface is accounted for. In real reactive absorption process, thermodynamic equilibrium is seldom reached, and real distillation and absorption process is a complex rate-controlled process that occurs far from thermodynamic equilibrium. Therefore, the equilibrium concept is often insufficient to describe and model it, and accurate and reliable models involving the process kinetics are required. Non-equilibrium model has been developed due to that reason.

This chapter reviewed and compared the equilibrium model and non-equilibrium model applied in reactive absorption.

3.1.1 Equilibrium model

The equilibrium model is the traditional way to analysis chemical absorption and desorption processes, which assumes that each gas stream leaving a tray or a packing segment (stage) is in thermodynamic equilibrium with the corresponding liquid stream leaving the same tray or segment. For reactive absorption, the chemical reaction must also be taken into account.

The entire column is divided into numbers of discrete stages as small segment demonstrated the equilibrium stage model in a counter-current column, where V donated vapor stream and L donated liquid stream. Thermodynamic equilibrium of equilibrium stage model is assumed to exist between the vapor and liquid streams leaving each stage. The equations applied in equilibrium model can be named as **MESH** equations, which collects the first capital letter of **M**aterial balances, **E**quilibrium relationships, **S**ummation equations and **H**eat/enthalpy balances (Taylor, Krishna et al. 2003).

The advantage of equilibrium stage model is so simple in concept that it has been used to simulate and design real columns. Each equilibrium stage represents an ideal tray. With very fast reactions, the equilibrium model can be satisfactorily applied in the reactive separation process. A proper modeling approach is based on the non-

reactive equilibrium stage model, which is extended by simultaneously considering the chemical equilibrium relations and the tray or stage efficiency. If the reaction rate is slower than the mass transfer rate, the influence of the reaction kinetics increases and becomes a dominating factor. The reaction kinetics has been integrated into the mass and energy balances in today's studies.

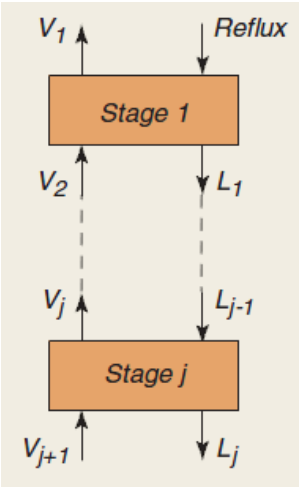

Figure 3-1 Decomposition of the distillation into stages (Taylor, Krishna et al. 2003)

However in fact, the streams leaving a real tray or section of a packed column are not in equilibrium with each other, which has been demonstrated in Figure 3-2. The separation depends on the rates of mass transfer from the vapor to the liquid phases (Taylor, Krishna et al. 2003). Therefore, correlation parameters such as tray efficiencies or height equivalent to a theoretical plate (HETP) are introduced to adjust the equilibrium-based theoretical description to real column conditions.

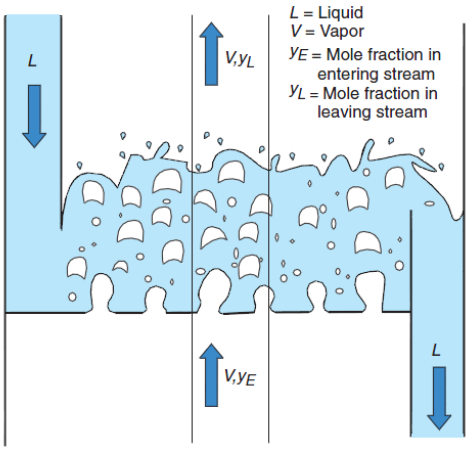

Figure 3-2 Flow patterns on a column tray (Taylor, Krishna et al. 2003).

For tray columns, different tray efficiencies have been used to describe the real trays from ideal trays in modelling and design. These efficiencies include the overall, Murphree, Hausen and vaporization(Taylor, Krishna et al. 2003). Murphree efficiency has been mostly admitted as a preference by many distillation experts (Taylor, Krishna et al. 2003), which is expressed as follow(Murphree 1925),

$$E_{Murph,i} = \frac{y_{iL} - y_{iE}}{y_{iL}^{*} - y_{iE}} \tag{3.1}$$

where, y_i indicates the mole fraction in stage i in entering (E) and leaving (L) stream, superscript * denotes equilibrium condition. The Murphree efficiency compares the actually absorbed amount in stage i to the maximum possible amount absorbed in stage i if the equilibrium is reached.

For packed columns, the packed bed is divided into a series of stages, and the number of equilibrium stages related to the real packed column is determined via HETP (Taylor, Krishna et al. 2003).

In fact, equilibrium stage model still has some major disadvantages. For example, correlation parameters vary from component to component and in a multicomponent mixture.

3.1.2 Non-Equilibrium Model

To overcome the limitation of equilibrium stage model, the more practical modelling of absorption and desorption has been developed, which is called as non-equilibrium model. The non-equilibrium model for reactive distillation follows the philosophy of rate-based models for conventional distillation (Krishnamurthy and Taylor 1985, Seader 1998), and considers actual rates of multicomponent mass and heat transfer and chemical reactions.

Several non-equilibrium models to incorporate mass and heat transfer have been proposed with different model complexity (Asprion 2006). The main differences among those non-equilibrium models are (i) the use of the driving force for the mass transfer, for example concentration gradient, chemical potentials, the electrochemical potentials and fugacity, and (ii) the diffusivity model, for example Fick's law or the Stefan-Maxwell approach.

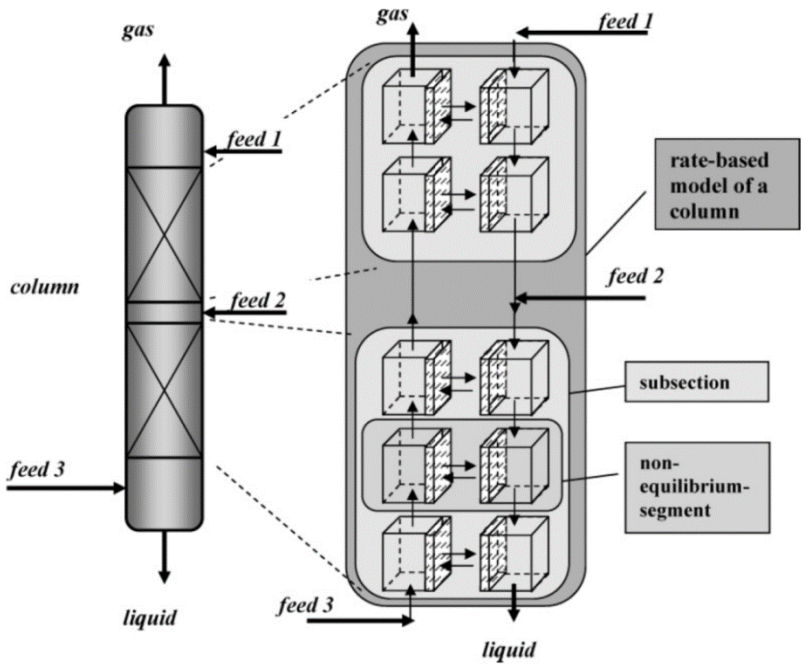

Figure 3-3 Rate-based model for a reactive distillation column (Asprion 2006)

Non-equilibrium model used to simulate mass and heat transfer in counter-current column is similar to the model of theoretical stages. As shown in Figure 3-3, the column is divided vertically into segments. In each of these non-equilibrium segments, mass and heat transfer occur between gas and liquid phases (Asprion 2006). The equations applied in rate-based model is referred to as the **MERSHQ** equations, which collects the first capital letter of **M**aterial balances, **E**nergy balances, mass- and heat-transfer **R**ate equations, **S**ummation equations, **H**ydraulic equations for pressure drop and **E**quilibrium equations (Taylor, Krishna et al. 2003).

The significant difference of non-equilibrium model from equilibrium model is that equilibrium only exists at the vapor – liquid interface, hence the separate balance equations have to be setup for each distinct phase (Taylor, Krishna et al. 2003). Figure 3-4 represents the mass- and energy transfer from vapor phase to liquid phase via interface. The challenges of non-equilibrium model are interfacial mass and energy transfers in tray and packed columns, which are used to determine the interfacial molar and energy fluxes. Therefore, the rate-based model is able to precisely describe the chemical absorption and desorption process.

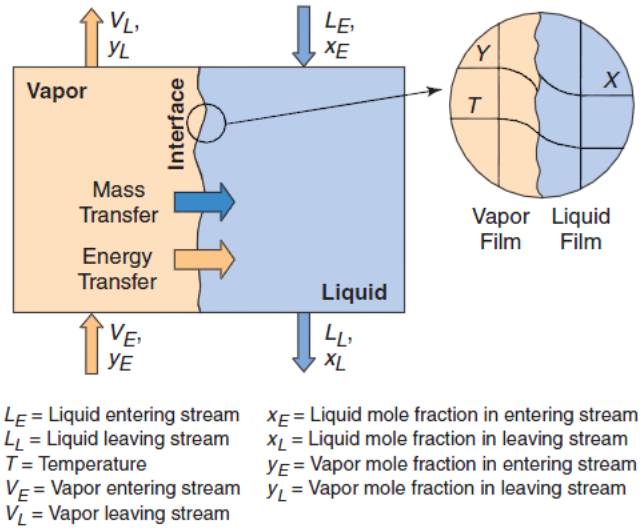

Figure 3-4 Schematic diagram of a non-equilibrium stage (Taylor, Krishna et al. 2003)

Mass and heat transfer at the gas-liquid interface can be described using different theoretical concepts. The common used models include the two-film model, surface renewal model and the film penetration theory. Those are described in detail in *chapter 3.4 mass transfer relations*. The model parameters are estimated via empirical correlations. In this work, a non-equilibrium model is presented that is based on the two-film model. The advantage of the two-film model is that there is a broad spectrum of correlations available in the literature for all types of column internals.

3.1.3 Comparison of equilibrium model and non-equilibrium model

Equilibrium model and non-equilibrium (or rate-based) model for reactive distillation were briefly presented above. The equilibrium models assume vapor-liquid equilibrium at each stage. The departure from equilibrium is accounted for by tray efficiency (tray columns) or the height equivalent of a theoretical plate (HETP). The rate-based models assume that the vapor-liquid equilibrium occurs only at the interface, and the Maxwell-Stefan equation is used to describe the mass transfer between the vapor phase and the liquid phase. The equations applied for equilibrium and non-equilibrium models are compared in Table 3-1.

Table 3-1 Comparison of equations between equilibrium and non-equilibrium model (Schneider and Gorak 2001, Ooi 2008)

	Equilibrium Stage Approach	Non-Equilibrium Rate-Based Approach
Stage Diagram:		
Material Balance:	$\frac{\partial M_{i,j}}{\partial t} = F_i \cdot z_{Fi,j} + G_{i+1} \cdot y_{i+1,j} + L_{i-1} \cdot x_{i-1,j} - G_i \cdot y_{i,j} - L_i \cdot x_{i,j}$	$\frac{\partial M_{Gi,j}}{\partial t} = F_{Gi} \cdot z_{GFi,j} + G_{i+1} \cdot y_{i+1,j} - G_i \cdot y_{i,j} - N_{Gi,j} \cdot a_{Ii} \cdot V_i$ $\frac{\partial M_{Li,j}}{\partial t} = F_{Li} \cdot z_{FLi,j} + L_{i-1} \cdot x_{i-1,j} - L_i \cdot x_{i,j} + N_{Li,j} \cdot a_{Ii} \cdot V_i$ $N_{Gi,j} = N_{Li,j}$
Equilibrium Relation:	$y_{i,j} = K_{i,j} \cdot x_{i,j}$	
Summation Equations:	$\sum_{j=1}^{NC} y_{i,j} = 1$ and $\sum_{j=1}^{NC} x_{i,j} = 1$	
Enthalpy Balance:	$\frac{\partial U_i}{\partial t} = F_i \cdot h_{Fi} + G_{i+1} \cdot h_{Gi+1} + L_{i-1} \cdot h_{Li-1} - G_i \cdot h_{Gi} - L_i \cdot h_{Li} - Q_i$	$\frac{\partial U_{Gi}}{\partial t} = F_{Gi} \cdot h_{FGi} + G_{i+1} \cdot h_{Gi+1} - G_i \cdot h_{Gi} - Q_{Gi} - E_{Gi} \cdot a_{Ii} \cdot V_i$ $\frac{\partial U_{Li}}{\partial t} = F_{Li} \cdot h_{FLi} + L_{i-1} \cdot h_{Li-1} - L_i \cdot h_{Li} - Q_{Li} + E_{Li} \cdot a_{Ii} \cdot V_i$ $E_{Gi} = E_{Li}$
Material Holdup:	$M_{i,j} = \left(y_{i,j} \cdot C_{Gfi} \cdot \phi_{Gi} + x_{i,j} \cdot C_{Lfi} \cdot \phi_{Li}\right) \cdot V_i$	$M_{Gi,j} = y_{i,j} \cdot C_{Gfi} \cdot \phi_{Gi} \cdot V_i$ $M_{Li,j} = x_{i,j} \cdot C_{Lfi} \cdot \phi_{Li} \cdot V_i$
Energy Holdup:	$U_i = \left(h_{Gi} \cdot C_{Gfi} \cdot \phi_{Gi} + h_{Li} \cdot C_{Lfi} \cdot \phi_{Li} - P_i\right) \cdot V_i$	$U_{Gi} = \left(h_{Gi} \cdot C_{Gfi} \cdot \phi_{Gi} - P_i\right) \cdot V_i$ $U_{Li} = h_{Li} \cdot C_{Lfi} \cdot \phi_{Li} \cdot V_i$
Stage Volume:	$V_i = \frac{\pi \cdot D_i^2 \cdot H_i}{4}$	
Stage Pressure:	$P_i = P_{i+1} - \Delta P_i$	

Notation: M is the component material holdup; F, G and L are the feed, vapour phase and liquid phase molar flow rates; N is the molar flux across the vapour-liquid interface; a_I is the effective interfacial area for mass transfer; x, y and z_F are the liquid phase, vapour phase and feed mole fractions; K is the equilibrium constant; NC is the number of components in the system; U is the energy holdup; h is the enthalpy; Q is the stage heat loss; E is the energy flux across the vapour-liquid interface; T is the temperature; C_t is the phase molar density; ϕ is the phase volumetric holdup; V is the stage volume; D is the stage diameter; H is the stage height; P is the stage pressure; and ΔP is the stage pressure drop. The subscripts F, G, L and I denote the feed, vapour phase, liquid phase and the vapour-liquid interface, while the subscripts i and j refer to stage i and component j.

Figure 3-5 represents the evolution of reactive absorption model. Starting from the classical equilibrium stage model on the bottom left, it assumes no reaction and infinitely fast mass transfer within the single stage. Then the equilibrium model has been developed by considering the bulk phase reaction kinetics and film reaction kinetics, which is shown on the bottom right. The equilibrium model accuracy and predictively gradually is improved due to the consideration of kinetically controlled reactions. Moving upwards, non-equilibrium models are introduced by taking into account mass transfer kinetics. The simplest rate-based model on the top left considers the chemical reaction to be at equilibrium when the reaction is fast. Furthermore, the enhancement fact has been introduced to study the cases where take place the chemical reaction in the liquid bulk (the top middle). The advanced rate-based model, shown on the top right, directly involved the process hydrodynamics via correlating the hole-up, pressure drop, mass transfer coefficients, etc (Kenig, Schneider et al. 2001).

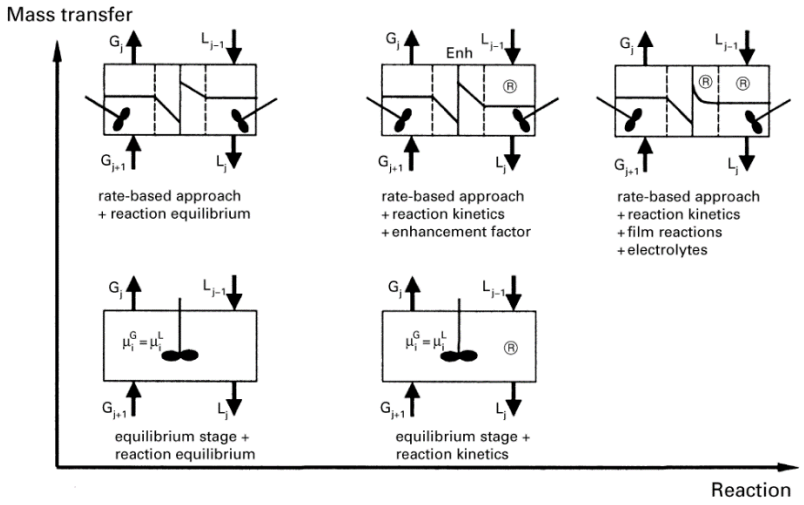

Figure 3-5 Reactive absorption model complexity (Kenig, Schneider et al. 2001)

Comparisons of steady-state equilibrium and rate-based models for reactive distillation have been studied in literatures (Lee and Dudukovic 1998, Baur, Higler et al. 2000, Peng, Lextrait et al. 2002). Lee and Dudukovic (1998) compared an equilibrium model with a rate-based model for a tray reactive distillation column. They concluded that the rate-based model was preferred as Murphree tray efficiency was difficult to predict priori. However, no available experimental data could support their conclusion that the rate-based model was preferred. Baur et al. (2000) compared an equilibrium model with a rate-based model for reactive distillation. They found that there were multiplicities in both the equilibrium model and the rate-based model.

However, the multiplicities observed by steady-state equilibrium model were much narrower than the multiplicities observed by the rate-based model. Peng et al. (2002) developed a steady-state equilibrium model and a rate-based model for a packed reactive distillation column. From their comparison, no major differences between the equilibrium model and the rate-based model have been observed for a range of simulation conditions. They found a relationship between the equilibrium models and the rate-based models. When the number of segments of column in the rate-based model is chosen to be the same as the number of the theoretical stages in the equilibrium model, and the vapor-liquid interface area is increased, the profiles from the rate-based model approach those from the equilibrium model.

The results predicted by the equilibrium and rate-based models are similar, and good agreement with experimental data. However, the rate-based model is much more complicated than the equilibrium model and more difficult to converge.

3.2 Chemical Reactions of CO_2 Absorption with Aqueous Alkanoamine Solutions

Amine is able to form soluble salts with the weak acids formed by H_2S and CO_2 in an aqueous solution. The reactions of amine and acid gases are high exothermic. H_2S reacts rapidly with the primary, secondary, or tertiary amine via a direct proton transfer reaction, regardless the structure of the amine (Kidnay 2011). However, the reaction between CO_2 and amine is much slower and more complex than H_2S, and it is amine structure dependence.

When CO_2 dissolved in water, carbonic acid is formed via hydroxylation, while bicarbonate is formed via slow dissociation. The bicarbonate then undergoes an acid-base reaction with amine, which occurs with any kinds of alkanolamine regardless the structure of amine, but the reaction mechanism of CO_2 with alkanolamine depends on amine structures.

All chemical reactions involved in CO_2 absorption by primary, secondary and tertiary alkanolamine are listed as follow,

Ionization of water

$$H_2O \leftrightarrow H^+ + OH^- \tag{3.2}$$

Hydroxylation of dissolved CO_2

$$CO_2 + H_2O \leftrightarrow H_2CO_3 \quad (3.3)$$

Dissociation of carbonic acid

$$H_2CO_3 \leftrightarrow H^+ + HCO_3^- \quad (3.4)$$

Dissociation of bicarbonate

$$HCO_3^- \leftrightarrow H^+ + CO_3^{2-} \quad (3.5)$$

Reaction of CO_2 with primary amine

$$R_1NH_2 + CO_2 \leftrightarrow H^+ + R_1HCOO^- \quad (3.6)$$

$$R_1NH_2 + H^+ \leftrightarrow R_1NH_3^+ \quad (3.7)$$

$$CO_2 + 2R_1NH_2 \leftrightarrow R_1HCOO^- + R_1NH_3^+ \ (overall\ reaction) \quad (3.8)$$

Reaction of CO_2 with secondary amine

$$CO_2 + R_1R_2NH \leftrightarrow H^+ + R_1R_2NCOO^- \quad (3.9)$$

$$R_1R_2NCOO^- + R_1R_2NH \leftrightarrow R_1R_2NCOO^- + R_1R_2NH_2^+ \quad (3.10)$$

$$CO_2 + 2R_1R_2NH \leftrightarrow R_1R_2NH_2^+ + R_1R_2NCOO^- \ (overall\ reaction) \quad (3.11)$$

Reaction of CO_2 with tertiary amine

$$CO_2 + H_2O + R_1R_2R_3N \leftrightarrow R_1R_2R_3NH^+ + HCO_3^- \ (overall\ reacton) \quad (3.12)$$

The reaction mechanism of CO_2 with primary or secondary amine is carbonate formation. The CO_2 reacts with one molecule of primary or secondary amine to form the carbonate intermediate, which reacts then with another amine molecule to form amine salt.

The reaction mechanism of CO_2 with tertiary amine is that an acid-base reaction of bicarbonate dissociated from carbonic acid with tertiary amine.

3.3 Chemical Reaction Kinetics Mechanisms

The reaction of CO_2 with primary, secondary and sterically hindered amines is described by the zwitterion mechanism and termolecular mechanism, whereas the reaction of CO_2 with tertiary amines is described by the based-catalyzed hydration mechanism (Vaidya and Kenig 2007).

3.3.1 Zwitterion Mechanism

Zwitterion mechanism is the typical mechanism that explains the reaction between CO_2 and primary, secondary and sterically hindered amines (Caplow 1968, Vaidya and Kenig 2007). Primary amine (denoted here as R_1NH_2) has been chosen as an example to briefly introduce zwitterion mechanism in following.

Step 1: Zwitterion formation

$$CO_2 + R_1NH_2 \overset{k_1}{\leftrightarrow} R_1NH_2^+COO^- \tag{3.13}$$

Step 2: Deprotonation

$$R_1NH_2^+COO^- \overset{k_B}{\rightarrow} R_1NH_2COO^- + BH^+ \tag{3.14}$$

According to the steady-state principle to the intermediate zwitterion, the rate of reaction of CO_2 in the aqueous solutions can be expressed as:

$$r = \frac{k_1(CO_2)(R_1NH_2)}{1 + \frac{k_{-1}}{k_B(B)}} \tag{3.15}$$

where $k_B(B)$ represents deprotonaton of the zwitterion by bases including H_2O, OH^-, amine, as well as mixture.

The reaction rate of CO_2 depends on the contribution of zwitterion reaction rate and deprotonaton reaction rate.

When the deprotonation reaction is instantaneous compared to the reverse reaction of zwitterion formation, i.e.$k_{-1} \ll k_B(B)$, the reaction rate of CO_2 can be expressed as:

$$r = k_1(CO_2)(R_1NH_2) \tag{3.16}$$

When the rate of reverse reaction of zwitterion formation is much faster than deprotonation reaction, i.e. $k_B(B) \ll k_{-1}$, the reaction rate of CO_2 can be expressed as:

$$r = \frac{k_1 k_B(B)}{k_{-1}}(CO_2)(R_1NH_2) \tag{3.17}$$

Carbamate formed via zwitterion mechanism may also undergo hydrolysis due to its low stability, forming bicarbonates and releasing one mole of free amine. Hydrolysis of carbamate can be expressed as:

$$R_1NH_2COO^- + H_2O \rightarrow HCO_3^- + R_1NH_2 \tag{3.18}$$

The free amine reacts with CO_2 again. The following reactions may occur simultaneously in an aqueous solution:

$$R_1NH_2 + H_2O \leftrightarrow R_1NH_3^+ + OH^- \tag{3.19}$$

$$H_2O \leftrightarrow H^+ + OH^- \tag{3.20}$$

$$CO_2 + OH^- \overset{k_{OH^-}}{\longleftrightarrow} HCO_3^- \tag{3.21}$$

$$CO_2 + H_2O \overset{k_{H_2O}}{\longleftrightarrow} HCO_3^- + H^+ \tag{3.22}$$

Thus, the total rate of all CO_2 reactions in an aqueous solution is the sum of the reaction rate corresponding to CO_2, which can be expressed as:

$$r_{overall} = \frac{k_1(CO_2)(R_1NH_2)}{1 + \frac{k_{-1}}{k_B(B)}} + \left\{\left[k_{H_2O}(H_2O) + k_{OH^-}(OH^-)\right](CO_2)\right\}$$

$$= k_{obs}(CO_2) \tag{3.23}$$

where, k_{obs} represents the observed reaction rate constant which is able to be calculated as following relation,

$$k_{obs} = \frac{k_1(R_1NH_2)}{1 + \frac{k_{-1}}{k_B(B)}} + \left[k_{H_2O}(H_2O) + k_{OH^-}(OH^-)\right] \tag{3.24}$$

Another term, the apparent reaction rate constant(k_{app}), is normally used to analyze during experimental measurement, where k_{H_2O} and k_{OH^-} can be neglected.

$$k_{app} = \frac{k_1(R_1NH_2)}{1 + \frac{k_{-1}}{k_B(B)}} \tag{3.25}$$

And the relation between k_{obs} and k_{app} is expressed as follow,

$$k_{app} = k_{obs} - \left[k_{H_2O}(H_2O) + k_{OH^-}(OH^-)\right] \quad (3.26)$$

3.3.2 Termolecular Mechanism

Termolecular mechanism is another mechanism which explains the reaction of CO_2 with primary, secondary and especially with sterically hindered amine(Crooks and Donnellan 1989). This mechanism assumes that the reaction proceeds in a single step via a loosely bound encounter complex as intermediate rather than zwitterion. The initial product of termolecular reaction mechanism of CO_2 with sterically hindered amine is demonstrated in Figure 3-6.

The reaction can be expressed as:

$$CO_2 + R_1NH_2 \cdots B \leftrightarrow R_1NH_2COO^- + BH^+ \quad (3.27)$$

The loosely-bound encounter complex breaks up to form reactant, while a small fraction reacts with a second molecule of amine, or a water molecule, to give ionic products. The reaction rate of CO_2 and amine for termolecular mechanism is

$$r = \left[k_{H_2O}(H_2O) + k_{OH^-}(OH^-) + k_{R_1NH_2}(R_1NH_2)\right](R_1NH_2)(CO_2) \quad (3.28)$$

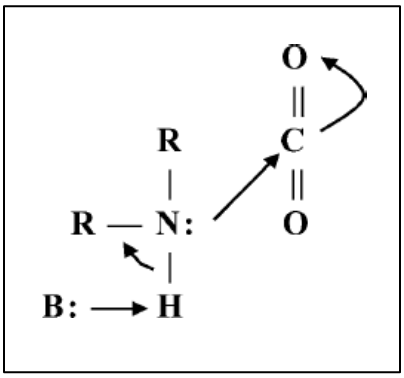

Figure 3-6 The initial product of termolecular reaction mechanism and carbonate formation (Ramachandran, Aboudheir et al. 2006)

3.3.3 Base-Catalyzed Hydration Mechanism

The reaction between CO_2 and tertiary amine can be described by base-catalyzed hydration mechanism. Because tertiary amine cannot react directly with CO_2, and it in fact undergoes an acid-base reaction following CO_2 hydroxylation and bicarbonate dissociation. The overall reaction is expressed as follow:

$$CO_2 + H_2O + R_1R_2R_3N \overset{k}{\leftrightarrow} R_1R_2R_3NH^+ + HCO_3^- \quad (3.29)$$

The reaction rate for base-catalyzed hydration mechanism is given by:

$$r = \left[k_{H_2O}(H_2O) + k_{OH^-}(OH^-) + k(R_1R_2R_3N)\right](CO_2) \quad (3.30)$$

3.4 Mass Transfer Relations

Different theoretical concepts about mass transfer at the gas-liquid interface have been performed to describe the behaviour of complicated interfacial mass transfer processes involving chemical reactions (Udani 1961). These theories include two-film model (Lweis 1924), penetration model (Higbie 1935) and Danckwerts surface renewal model (Danckwerts 1951).

3.4.1. Film theory

Two-film theory was first suggested by Whitman (1923) and by Lewis and Whitman (1924). In two-film model, stationary vapour and liquid films are postulated to form on the both sides of vapour-liquid interface, as sketched in Figure 3-7. CO_2 in the vapour bulk passes through the vapour film, then enters the liquid film after crossing vapour-liquid interface where the reactions between CO_2 and amine start. All resistances to mass transfer are assumed to be concentrated in two films. Mass transfer relations are only limited by liquid film (Yih 1987). Additionally, since the thickness of films is extremely thin, mass transfer within the films is only droved by concentration gradient due to steady-state molecular diffusion (Taylor 1993). Physical equilibrium exists at the interface, whereas chemical equilibrium takes place in the bulk phases where components are mixed completely (Taylor 1993).

The mass transfer relations can be described by different theoretical equations. Maxwell-Stefan equation is the most rigorous due to considering the component diffusion fluxes to chemical and electrical potential gradients (Taylor 1993). Fick's law has been used to simplify Maxwell-Stefan equation by assuming that the system is sufficiently dilute that the diffusional interactions between the components can be ignored. Especially, some studies have shown also that the effects of electrical potential gradient on mass transfer relations of CO_2 removal processes are negligible (Schneider and Gorak 2001, Ooi 2008). The Fick's law has been applied in mass transfer simulation in this work.

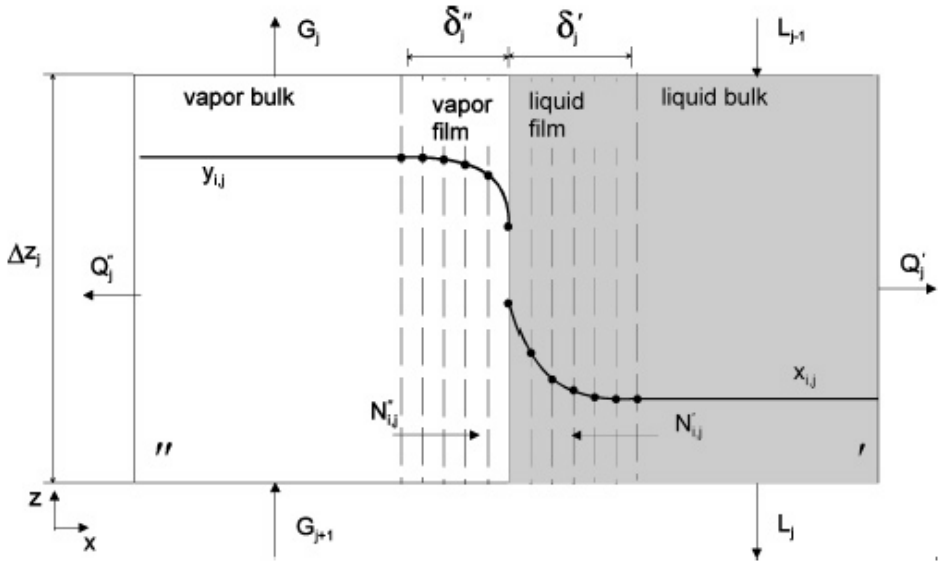

Figure 3-7 The two-film model for the mass transfer for non-equilibrium segment (Asprion 2006)

The mass transfer equation in physical absorption is determined from the mass balance of the solute at steady state as

$$D_A \frac{\partial^2 C_A}{\partial x^2} = 0 \qquad for\ 0 \le x \le \delta \tag{3.31}$$

For the mass transfer equation cooperated with chemical reaction, eq (3.32) is replaced by

$$D_A \frac{\partial^2 C_A}{\partial x^2} = r(x) \qquad for\ 0 \le x \le \delta \tag{3.32}$$

The boundary conditions are

$$When\ x = 0, \quad C_A = C_{A,i}$$

$$When\ x = \delta, \quad C_A = C_{A,b}$$

The mass transfer flux will then be

$$N_A = -D_A \frac{dC_A}{dx} = \frac{D_A}{\delta}\left(C_{A,b} - C_{A,i}\right) = k_l(C_{A,b} - C_{A,i}) \tag{3.33}$$

where k_l denotes the mass transfer coefficient for liquid side,

$$k_l = \frac{D_A}{\delta} \tag{3.34}$$

Mass fluxes across the vapour-liquid interface can be calculated by following equations,

Gas

$$N_{Gi} = -D_{Gi}\frac{dP_{Gi}}{dx} = -D_{Gi} \cdot P_G \cdot \frac{dy_i}{dx} \tag{3.35}$$

Liquid

$$N_{Li} = -D_{Li}\frac{dC_{Li}}{dx} = -D_{Li} \cdot C_L \cdot \frac{dx_i}{dx} \tag{3.36}$$

3.4.2. Film Penetration Theory

The film-penetration theory adopts the unsteady state molecular diffusion mechanism. Higbie was first who came up with the film penetration theory based on the hypothesis that, liquid-gas interface is composed of tiny liquid elements that are incessantly brought to the surface from bulk of the liquid (Higbie 1935). These elements are considered as stagnant. When liquid element reached the surface, the dissolved gas concentration in the element is supposed to be equal to the liquid bulk concentration. Therefore mass transfer is presented as follow:

$$D_A\frac{\partial^2 C_A}{\partial x^2} = \frac{\partial C_A}{\partial t} \tag{3.37}$$

Initial and boundary conditions:

$$C_A(0,t) = C_{A,i}$$

$$C_A(\infty,t) = C_{A,b}$$

$$C_A(x,0) = 0$$

The mass transfer rate with above conditions gives a solution:

$$N_A = k_l(C_{A,i} - C_{A,b}) \tag{3.38}$$

where k_l denotes the mass transfer coefficient

$$k_l = 2\sqrt{\frac{D_A}{\pi t}} \tag{3.39}$$

3.4.3. Surface Renewal Model

Surface renewal model for mass transfer was proposed by Danckwerts as extension of film penetration theory (Danckwerts 1951). It is based on the assumption that the liquid elements do not stay on the surface (gas-liquid contact) at the same time. It is the complex model of fluid mechanics. In surface renewal model, the interface is observed as being formed by a number of elements, and each one of which has been brought to the surface some time t before the instant of observation. The distribution of the surface element contact times is described by a distribution function

$$\psi(t) = se - st \tag{3.40}$$

where

$$\psi(t) = \frac{1}{t^*} \qquad for\ t < t^*$$

and

$$\psi(t) = 0 \qquad for\ t > t^*$$

The absorption rate at the surface stated by Danckwerts' age function is:

$$N_A(t) = C_{A,i}\sqrt{D_A(k_l + s)} = C_{A,i}\sqrt{D_A(k_l + \frac{k_l^2}{D_A})} = k_l \cdot C_{A,i}\sqrt{1 + \frac{D_A}{k_l}} \tag{3.41}$$

where

$$k_l = \sqrt{D_A \cdot s} \tag{3.42}$$

3.5 Energy Transfer Relations

The two-film model is able to describe the energy transfer across the vapour - liquid interface. All resistances to the energy transfer are assumed to be concentrated in both vapour and liquid films attaching on either side of the interface. The energy transfer relations within two films are assumed to take place only by steady-state heat conduction driven by the temperature gradient. Both phases are in thermal equilibrium at the interface. That is to say that the vapour temperature equals to the liquid temperature at the interface and keep uniform in both bulk phases (Ooi 2008).

The energy fluxes across the vapour-liquid interface can be analogous to Fick's law (Taylor 1993, Ooi 2008), and consist of conductive heat fluxes and the convective contributions. The equations of energy transfer relations are represented as following,

Gas

$$E_G = -\alpha_G \frac{dT_G}{dz} + \sum N_{Gi} \cdot h_{Gi} \tag{3.43}$$

Liquid

$$E_L = -\alpha_L \frac{dT_L}{dz} + \sum N_{Li} \cdot h_{Li} \tag{3.44}$$

3.6 Chemical Reactions

Since chemical reactions involved in CO_2 absorption process using alkanolamine solutions, the effects of chemical reactions on mass/energy transfer have to be taken into account. These have been addressed in this sub-chapter, including chemical equilibrium relations, reaction rate and enhancement factor.

3.6.1 Chemical equilibrium relations

The calculation of chemical equilibrium is similar as the calculation of phase equilibrium. Whether the system is in equilibrium situation can be determined by one of the following four ways, Internal Energy (U), Enthalpy (H), Helmholtz Free Energy (A) and Gibbs Free Energy (G). G is the common method to determine the phase equilibrium, because it only requires the simplest measurable properties temperature and pressure. G is minimized at equilibrium

$$\partial G = \sum_{i=1}^{n} \mu_i \partial n_i = 0 \tag{3.45}$$

where μ_i represents the chemical potential of component i in the system that can be expressed as

$$\mu_i = \mu_i^0 + RTln(\gamma_i x_i) \tag{3.46}$$

where $\gamma_i$represents the activity coefficient of component i in the system that can be expressed as

$$\gamma_i = \frac{\varphi_i(T, P, x_i)}{\varphi_i(T, P, x_i \to 0)} \tag{3.47}$$

where φ_i represents the fugacity coefficient of component i in the system that can be expressed as

$$\varphi_i = \frac{f_i}{P_i} \tag{3.48}$$

where f_i represents the fugacity of component i in the system.

A homogenous chemical reaction

$$\vartheta_{R1}R_1 + \vartheta_{R2}R_2 + \cdots + \vartheta_{Rn}R_n \to \vartheta_{P1}P_1 + \vartheta_{P2}P_2 + \cdots + \vartheta_{Pm}P_m \tag{3.49}$$

The chemical equilibrium relations is shown by following equation

$$K_{eq} = \frac{\prod_i^m (x_{Pi} \cdot \gamma_{Pi})^{\vartheta_{Pi}}}{\prod_j^n (x_{Ri} \cdot \gamma_{Ri})^{\vartheta_{Ri}}} \tag{3.50}$$

where, R and P denote the reactant and product respectively, ϑ is the stoichiometric coefficient, γ is the activity coefficient, x is the mole friction, $K_{eq}$is the mole-friction equilibrium constant.

For the fast or instantaneous reactions, the effects of chemical reactions on the rate of mass transfer can be described by the chemical equilibrium relations, whereas the

chemical equilibrium relations are not adequate for the slow or kinetically controlled reactions, thus the reaction rate expressions or enhancement factors have to be considered.

3.6.2 Reaction rate

For slow or kinetically controlled reactions, the reaction rate r has been successfully applied in a number of non-equilibrium rate-based models of acid gas absorption processes (Mayer, Schneider et al. 1999, Kucka, Muller et al. 2003, Ooi 2008). All kinetically relations have been reviewed in chapter 3.3. Moreover, the reaction rate r can be used either over an entire phase or within the film region. In this thesis work, the effects of the chemical reactions on mass transfer have been described by reaction rate.

3.6.3 Enhancement factor

The effect of slow or kinetically controlled reactions on the rate of mass transfer can also be addressed by enhancement factor. Enhancement factor describes the acceleration of the interfacial diffusion fluxes due to chemical reactions.

Enhancement factor is expressed as

$$E = \sqrt{1 + Ha^2} \tag{3.51}$$

where, Ha is Hatta number that is expressed as following,

$$Ha = \frac{\sqrt{k \cdot D}}{k_l} \tag{3.52}$$

where, k is the first-order or pseudo-first-order reaction rate constant, k_l is the liquid phase mass transfer coefficient.

From the expression of Hatta number, it is the ratio between the maximum rate of reaction in the liquid film and the maximum rate of mass transfer through the liquid film (Sharma and Danckwer.Pv 1970). Thus, the reaction kinetic regime can be categorized corresponding to Hatta number,

- $Ha < 0.3$ Slow reactions, and occur only in the liquid bulk phase
- $Ha > 3$ Fast reactions, and complete within the liquid film
- $0.3 < Ha < 3$ Moderately fast reactions, and happen in both the liquid bulk phase and the liquid film.

According to the definition of enhancement factor, it can be expressed as the ratio between mass transfer flux accelerated by chemical reactions and mass transfer flux only due to physical absorption. The enhancement factor can calculated as following,

$$E = \frac{Flux}{k_l^0 \cdot ([CO_2]_i - [CO_2]^*)} \tag{3.53}$$

where, $[CO_2]_i$ is the concentration of CO_2 at the interface, $[CO_2]^*$ is the real concentration of CO_2 in the liquid phase, k_l^0 is the liquid phase mass transfer coefficient.

3.7 Mass and Heat Transfer Coefficient

The simulation of non-equilibrium model of CO_2 absorption in alkanolamines requires the mass and heat transfer coefficients, which has been reviewed as following.

3.7.1. Mass Transfer Coefficient

It is necessary to consider the gas and liquid film resistance accurately describe the mass transfer between gas and liquid phases. The mass transfer coefficients of each component in gas and liquid film represent the film resistance.

The total resistance $(1/K_G)$ to mass transfer between the gas and liquid phases in associated with chemical reactions is the sum of gas film resistance $(1/k_g)$ and liquid film resistance $(1/k_G')$, the relation is expressed as follow,

$$\frac{1}{k_g} + \frac{1}{k_G'} = \frac{1}{K_G} \tag{3.54}$$

The total mass transfer coefficient, K_G, can be calculated by the following expression,

$$K_G = \frac{Flux}{P_{CO_2} - P_{CO_2}^*} \tag{3.55}$$

where, $P_{CO_2}^*$ represents the equilibrium partial pressure of CO_2, P_{CO_2} is the operational partial pressure of CO_2 that can be calculated by the log mean average,

$$P_{CO_2} = \frac{P_{CO_2,in} - P_{CO_2,out}}{\ln(P_{CO_2,in}/P_{CO_2,out})} \tag{3.56}$$

The liquid phase mass transfer coefficient with chemical reactions, k'_G, can be calculated by following expression,

$$k'_G = \frac{Flux}{P_{CO_2,i} - P^*_{CO_2}} \tag{3.57}$$

where, $P_{CO_2,i}$ is the partial pressure of CO_2 at interface which can be calculated by

$$P_{CO_2,i} = P_{CO_2} - \frac{Flux}{k_g} \tag{3.58}$$

The liquid phase mass transfer coefficient with chemical reactions, k'_G, can be calculated by another expression,

$$k'_G = \frac{k_l^o \cdot E}{H_{CO_2}} = \frac{\sqrt{k_{obs} \cdot D_{CO_2}}}{H_{CO_2}} \tag{3.59}$$

The gas phase mass transfer coefficient, k_g, can be determined by a dimensionless formula showing as following (Bishnoi and Rochelle 2000),

$$Sh = \alpha(Re \cdot Sc \cdot d/h)^{\beta} \tag{3.60}$$

where, Sherwood number $Sh = \frac{RTk_g d}{D_{CO_2}}$, Reynolds number $Re = \frac{\rho v d}{\mu}$, Schmidt number $Sc = \frac{v}{D}$, d is hydraulic diameter of the column, h is height of the column, parameters α and β depend on the equipment that should be determined by experiment.

3.7.2. Heat transfer coefficient

The gas and liquid film resistance to energy transfer is described by the gas and liquid heat transfer coefficient. In the two-film model, it is assumed that the films are stagnating. Thus, only diffusive mass transfer and no convective mass transfer are taken into account. The consequent use of the two-film model would be to allow only for heat conduction. Chilton-Colburn analogy is an approach that applies the mass/heat transfer analogy to estimate the heat transfer coefficient for the gas and liquid (Bird 1960, Pacheco and Rochelle 1998).

$$Nu = Le^{-1/3} \cdot Sh \tag{3.61}$$

or

$$Nu = \alpha(Re \cdot Pr)^{\beta} \tag{3.62}$$

where, Nu denotes Nesselt number, Le denotes the Lewis number, Sh denotes the Sherwood number, Re denotes the Reynolds number and Pr represents Prandtl number.

For the two film model, the film thickness, δ, of the mass transfer is correlated with the mass transfer coefficient, K_G, and the diffusion coefficient, D:

$$\delta = \frac{D}{K_G} \tag{3.63}$$

Then the relation comes out from Chilton-Colburn analogy:

$$\alpha = Le^{-\frac{1}{3}}(\frac{\lambda}{\delta}) \tag{3.64}$$

where, α denotes the heat-transfer coefficient, λ denotes the heat conductivity.

The Lewis number is in the order of magnitudes of 10-100 for liquids and is in the range of 0.7-3 for gases (Asprion 2006). Hence, the relations between heat-transfer coefficient and heat conductivity for gas and liquid film can be rewrote as

Gas

$$\alpha_G = (0.9\ to\ 1.4) \times (\frac{\lambda_G}{\delta_G}) \tag{3.65}$$

Liquid

$$\alpha_L = (\frac{1}{2}\ to\ \frac{1}{5}) \times (\frac{\lambda_L}{\delta_L}) \tag{3.66}$$

From the above two relations, we can see that for the liquid, the heat transfer resistance is higher for the Chilton-Colburn analogy, in comparison to the heat conduction. For gas, there is only a small difference. In another word, the heat transfer coefficients of liquid components do not significantly affect the temperature profile, whereas the heat transfer

coefficients of vapor components dominate the accuracy of temperature profile simulation (Pacheco and Rochelle 1998).

Given the definition of temperature boundary layer thickness,

$$\delta_T = \frac{\lambda}{\alpha} \tag{3.67}$$

It is obvious that the thickness of the temperature boundary layer of the liquid is 2-5 times greater than the diffusion film thickness. For the gas, both layers have almost the same thickness. As shown by the investigations of Frank et al.(Frank, Kuipers et al. 1995, Frank, Kuipers et al. 1995) , it is important to account for the heat effects; however, the influence of the Lewis number is less essential and generally does not seem to be critical. In most cases, the heat transfer in the liquid is not the determining factor, so there is not a great difference between using the heat transfer coefficient and the heat conductivity. In this work, the heat conductivity is used, because the same film thickness for heat and mass transfer is used.

4. Modeling of CO_2 Absorption with MEA

4.1 Model Parameters

Physic-chemical properties of the fluids are required when modeling or simulating mass and energy transfer in reactive absorption process. These include density, viscosity, diffusivity, solubility, reaction rate constants, mass/heat transfer coefficient and specific heat capacity of all components presented in the system.

4.1.1. Density

The density of aqueous MEA solution was calculated according to the correlation developed by Weiland et al.(Weiland, Dingman et al. 1998).

4.1.2. Diffusivity

The N_2O analogy was used to determine the diffusivity of CO_2 in amine solutions. The diffusivity of N_2O in MEA was calculated from the simple correlation developed by Ko et al. (Ko, Tsai et al. 2001). On the other hand, the diffusivity of MEA in the aqueous MEA solutions was calculated from the correlation developed by (Snijder, Teriele et al. 1993).

1) Diffusivity coefficient of CO_2 in amine solutions

The free molecular diffusivity of CO_2 in amine solutions can be estimated correctly from the N_2O analogy, and the relation is illustrated as follow,

$$D_{CO_2} = D_{N_2O} \cdot (D_{CO_2}/D_{N_2O})_{in\ water} \tag{4.1}$$

The empirical equations of the diffusivity of N_2O and CO_2 in water have been proposed by Versteeg and Vanswaaij, and shown as follow respectively (Versteeg and Vanswaaij 1988),

$$D_{N_2O}[m^2/s] = b_0 exp\{-2371/T[K]\} \tag{4.2}$$

$$D_{CO_2}[m^2/s] = b_5 exp\{-2119/T[K]\} \tag{4.3}$$

Diffusivity of N_2O in MEA has been estimated via a simple developed correlation, which is shown as follow,

$$D_{N_2O}[m^2/s] = \{b_0 + b_1 C_{amine}[kmol/m^3] + b_2 C_{amine} \times \exp\{b_3 + b_4 C_{amine}/T[K]\}$$

(4.4)

where, the number of parameters in diffusivity equation for aqueous alkanolamine solutions were listed in Table 4-1 (Ko, Tsai et al. 2001).

Table 4-1 Parameters in diffusivity equation for aqueous alkanolamine solutions

Parameter	Number
b_0	5.07×10^{-6}
b_1	8.65×10^{-7}
b_2	2.78×10^{-7}
b_3	-2371
b_4	-93.4
b_5	2.35×10^{-6}
b_6	-2119

2) Diffusivity coefficient of aqueous alkanolamine solutions

The diffusivity of MEA in aqueous amine solutions was determined from the correctly development of Taylor dispersion technique (Snijder, Teriele et al. 1993), which has been corrected as the function of operational temperature and concentration of MEA aqueous solutions. The corrected diffusivity coefficient of aqueous MEA solution is represented as follow under typical operational conditions where temperature ranges from 298 to 333 K and amine solution concentration ranges from 0.043 to 5.016 $kmol/m^3$,

$$ln(D_{MEA}) = -13.275 - 2198.3/T - 7.8142 \times 10^{-2} C_{MEA} \quad (4.5)$$

4.1.3. Solubility and Henry's Law Constant

The Henry's law constant of CO_2 in aqueous alkanolamine solutions can be calculated from the Henry's law constant of N_2O in the same solvent according to N_2O analogy (Clarke 1964), and the relation is illustrated as follow,

$$H_{CO_2} = H_{N_2O} \cdot (H_{CO_2}/H_{N_2O})_{in\ water} \quad (4.6)$$

The Henry's law constant of N_2O and CO_2 in water as a function of temperature is shown as follow (Penttila, Dell'Era et al. 2011),

$$H_{gas,water}[Pa \cdot m^3/mol] = \exp\{a + \frac{b}{T[K]} + c \cdot lnT + d \cdot T\} \quad (4.7)$$

Parameters of the above equation for Henry's law constant of N_2O and CO_2 were listed in Table 4-2.

Table 4-2 Parameter for Henry's law constant of N_2O and CO_2 in water, and of N_2O in pure MEA (Penttila, Dell'Era et al. 2011)

Henry's law constant	a	b	c	d	Temperature [K]
$H_{N_2O,water}$	158.245	-9048.596	-20.860	-0.00252	283.15-413.15
$H_{CO_2,water}$	145.369	-8172.355	-19.303	0	273.15-433.15
$H_{N_2O,MEA}$	-9172.50	39.598			293.55-356.85

The equation for calculating the Henry's law constant of of N_2O in pure amine is given as follow, where the corresponding parameters are listed in Table 4-2.

$$H_{N_2O,amine}[Pa \cdot m^3/mol] = a + b \cdot T \quad (4.8)$$

The Henry's law constant of of N_2O in aqueous alkanolamine solution was calculated by a semi-empirical equation, which was the function of temperature and solvent composition (Penttila, Dell'Era et al. 2011).

$$H_{N_2O,amine-water}[Pa \cdot m^3/mol] = \sum H_{N2O,i} \cdot x_i + A\left(\prod x_i\right)^2 (1 - \frac{T[K]}{B})\exp(-C_{MEA}) \quad (4.9)$$

where, *i* represents each component in aqueous alkanolamine solution, and A, B, C represent the parameters fitted to the Henry's law constant data of aqueous alkanolamine solvents which have been listed in Table 4-3.

Table 4-3 Parameters for the Henry's law constant of of N_2O in aqueous alkanolamine solutions (Penttila, Dell'Era et al. 2011)

Solvent system	A	B	C
MEA-water	3524641.533	324.718	13.219

4.1.4. Reaction Rate Coefficient of CO_2 with Aqueous MEA Solution, k

Reaction rate coefficient between CO_2 and aqueous MEA solution was calculated by following equation,

$$k = 4.61 \times 10^9 \exp(-\frac{4412}{T}) \tag{4.10}$$

This reaction rate coefficient equation is able to be applied in the reaction conditions where the temperature is in range from 293 to 333 K, and MEA concentration is in range from 3-9 kmol/m^3(Aboudheir, Tontiwachwuthikul et al. 2003).

4.1.5. Heat Capacity of Aqueous MEA Solutions Blending with CO_2, C_p

The heat capacity of aqueous MEA solutions blending with CO2 was determined according to Weiland et al. (Weiland, Dingman et al. 1997), Table 4-4 listed the heat capacity of aqueous MEA solutions with CO_2 loading.

Table 4-4 Heat Capacity ($kJ/kg \cdot K$) of CO_2-loaded MEA solutions at 298 K

Loading (mol/mol)	10 mass % MEA	20 mass % MEA	30 mass % MEA	40 mass % MEA
0.00	4.061	3.911	3.734	3.634
0.05	4.015			
0.10		3.823	3.656	3.508
0.20	3.917	3.766	3.570	3.343
0.30	3.915	3.670	3.457	3.238
0.40	3.891	3.648	3.418	3.163
0.50	3.857	3.597	3.359	3.109

4.1.6. Enthalpies of Solutions of CO_2 in Aqueous MEA Solution

The enthalpies of solution of CO_2 in aqueous MEA solutions were determined by experimental data measured by Arcis (Arcis, Ballerat-Busserolles et al. 2011).

4.1.7. Heat Transfer Coefficient and Thermal Conductivity

Thermal conductivities have been used in this work for simplifying the calculation, since the same film thickness for temperature and mass transfer can be used. Moreover in most cases, the heat transfer in the liquid is not the determine factor, so there is not a great difference between using the heat transfer coefficient and the thermal conductivities.

No experimental data have been published about the thermal conductivity and diffusion coefficients of CO_2/Amine/H_2O mixtures (Hailong Li). Hence, the thermal conductivity of aqueous MEA solutions was used in this work and calculated by equation:

$$\lambda\ [kW/m \cdot K] = \sum x_i \cdot \lambda_i \tag{4.11}$$

where, x_i denotes the molar fraction of each component in the system, λ_i denotes the thermal conductivity of the corresponding component (see Table 4-5).

Table 4-5 Thermal conductivities of pure MEA and water (Peyghambarzadeh, Jamialahmadi et al. 2009)

	Thermal conductivity, [kW/m K]
Water	0.676
MEA	0.22

4.2 Review of Project Model

In the semester project, the mass transfer of CO_2 absorption by using aqueous MEA solution was simulated. Two-film model was used, and the CO_2 concentration was calculated by numerical matrix calculation using MATLAB.

Figure 4-1 demonstrates the sketch of two-film model used in project. The mass fluxes of CO_2 in the liquid film was analysed from gas – liquid interface ($z = 0$) to the liquid film – liquid bulk interface ($z = \delta$). The liquid film was divided into *n* equal segment grids. The components in each segment were assumed to be the same. The components in the liquid phase were assumed consist of MEA, water and CO_2.

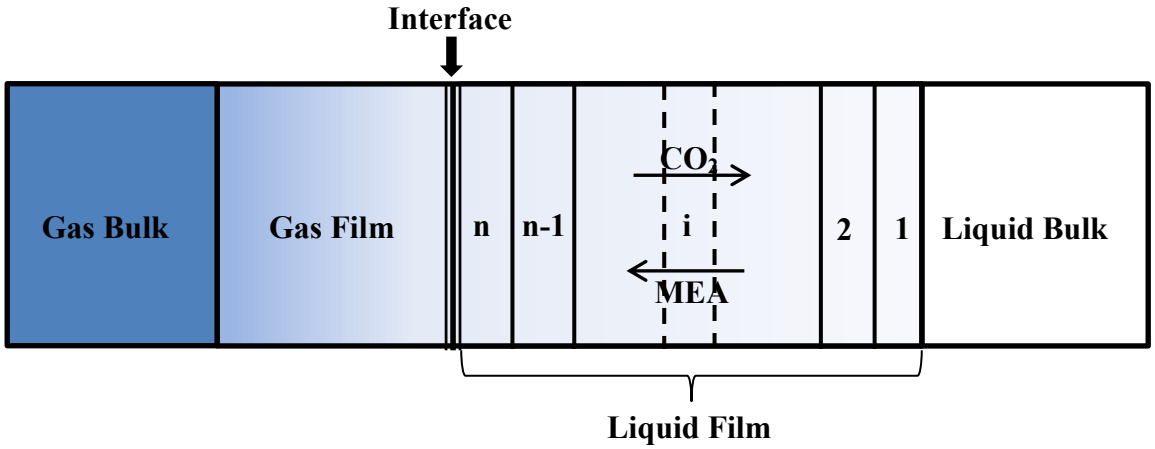

Figure 4-1 Sketch of two-film model applied in the semester project

The mass transfer relation in each segment was set based on that the diffusive mass flux equalled to the mass flux of corresponding component consumed during chemical reaction:

$$[\boldsymbol{Flux\ change}] = [\boldsymbol{Kinetics\ reaction\ rate}] \times [\boldsymbol{Thinkness\ of\ each\ segment}] \tag{4.12}$$

The mass balance equations for CO_2 in liquid film were set by equation 4.12. There should be noticed that mass balance equations in segment 1 and segment n were special due to boundary conditions.

Segment 1,

CO_2 concentration in liquid bulk was assumed equal to 0

$$D_{CO_2}\left(\frac{[CO_2]_b - [CO_2]_1}{\Delta z}\right) - D_{CO_2}\left(\frac{[CO_2]_1 - [CO_2]_2}{\Delta z}\right) = k_{MEA}[CO_2]_1[MEA]_1\Delta z \tag{4.13}$$

Segment 2 to n-1,

General term in matrix calculation

$$D_{CO_2}\left(\frac{[CO_2]_{m-1} - [CO_2]_m}{\Delta z}\right) - D_{CO_2}\left(\frac{[CO_2]_m - [CO_2]_{m+1}}{\Delta z}\right) = k_{MEA}[CO_2]_m[MEA]_m\Delta z \tag{4.14}$$

Segment n,

CO_2 concentration in segment n equalled to CO_2 concentration at gas-liquid interface, which was expressed from Henry's Law.

$$[CO_2]_n = [CO_2]_i = \frac{P_{CO_2}}{H_{CO_2}} \tag{4.15}$$

4.3 Mass Transfer in Liquid Film

In this thesis work, two-film model was used. The mass transfer relations were determined according to Eq 3.32, and the chemical equilibrium was taken into account. The coupled differential equations were solved by using BVP4C MATLAB solver.

$$D_{CO_2} \frac{d^2[CO_2]}{dx^2} = k_{MEA} \cdot [MEA] \cdot [CO_2] \tag{4.16}$$

$$D_{MEA} \frac{d^2[MEA]}{dx^2} = 2 \cdot k_{MEA} \cdot [MEA] \cdot [CO_2] \tag{4.17}$$

with boundary conditions

For CO_2

$$when\ x = 0, \qquad [CO_2]_i = \frac{P_{CO_2}}{H_{CO_2}}$$

$$when\ x = \delta, \qquad \frac{d[CO_2]}{dx} = 0$$

For MEA

$$when\ x = 0, \qquad \frac{d[MEA]}{dx} = 0$$

$$when\ x = \delta, \qquad [MEA] = [MEA]_b$$

4.4 Evaluation of Temperature Gradient in Liquid Film

In each film segment, heat released due to chemical reaction was calculated by

$$Q = r \cdot \Delta H \cdot \Delta V = k_{MEA} \cdot [MEA] \cdot [CO_2] \cdot \Delta H \cdot \Delta V \tag{4.18}$$

where, Q denotes chemical reaction heat, ΔH denotes the enthalpy of CO_2 absorption reaction, and ΔV denotes the reaction volume. Here, we assumed the reaction volume was a cube with 1m long, 1m height and dx width. So the reaction heat in each segment can be rewrote as

$$dQ = k_{MEA} \cdot [MEA] \cdot [CO_2] \cdot \Delta H \cdot dx \tag{4.19}$$

Temperature gradient in liquid film was determined based on equation

$$Q = m \cdot C_p \cdot \frac{dT}{dt} \tag{4.20}$$

where, m is the mass in reaction volume ΔV, and $m = \rho \Delta V$, C_p denotes the specific heat capacity of aqueous MEA solutions.

According to above, temperature gradient in the liquid film was calculated by

$$\frac{dT}{dt} = \frac{k_{MEA} \cdot [MEA] \cdot [CO_2] \cdot \Delta H}{\rho \cdot C_p} \tag{4.21}$$

4.5 Heat Transfer in Liquid Film

Thermal conductivities have been used in this thesis work, since the same film thickness for temperature and mass transfer can be used, which simplified the calculation.

The energy balance consists of the incoming and outcoming enthalpy stream and heat flux. There are no source terms, because the heat of reaction is included in the partial molar enthalpies. The calculation of energy equation was incorporated with mass transfer equations as presented in chapter 4.3, and BVP4C MATLAB Solver was used for calculation.

$$\lambda \frac{dT}{dx} + \sum (N_i \cdot h_i) = 0 \tag{4.22}$$

where, h_i denotes the enthalpy for each component, and N_i denotes molar flux and the expressions of reaction rate are substituted by Eq 3.32 and Eq 3.33,

$$N_{CO_2} = r_{CO_2} \cdot dx = k_{MEA} \cdot [MEA] \cdot [CO_2] \cdot dx \tag{4.23}$$

$$N_{MEA} = r_{MEA} \cdot dx = 2 \cdot k_{MEA} \cdot [MEA] \cdot [CO_2] \cdot dx \tag{4.24}$$

then, the energy equation is rewrote as

$$\lambda \frac{d^2T}{dx^2} + (r_{CO_2} \cdot h_{CO_2} + r_{MEA} \cdot h_{MEA}) = 0 \tag{4.25}$$

with boundary conditions

$$when\ x = 0, \qquad \frac{dT}{dx} = 0$$

$$when\ x = \delta, \qquad T = T_b$$

where, T_b denotes the initial operation temperature in unit K.

5. Results

5.1 CO_2 concentration profile and comparison of BVP4C results with project results

In this thesis, a non-equilibrium model is presented that is based on two-film model. Table 5-1 lists the values of initial parameter inputs for modeling. The physic-chemical properties used for simulation are presented in Table 5-2.

Table 5-1 Initial parameter inputs used for simulation

Parameter	Value
Film thickness	$5 \times 10^{-6}\ m$
Temperature	298 K
Pressure	10 kPa
CO_2 partial pressure, y_{CO_2}	1.0
CO_2 loading, α	0
MEA mass weight, *wt%*	30%

Table 5-2 Physic-chemical properties used for simulation

Parameters		Value
Reaction rate constant	k	$1662.2\ s^{-1}$
Diffusivity of CO_2	D_{CO_2}	$1.2903 \times 10^{-9}\ m^2/s$
Diffusivity of MEA	D_{MEA}	$0.7266 \times 10^{-9}\ m^2/s$
Henry's law constant of CO_2	H_{CO_2}	$1919.1\ kPa \cdot m^3/kmol$
Heat conductivity of MEA	D_{CO_2}	$0.624 \times 10^{-3}\ kW/(m \cdot K)$
Heat capacity of MEA	C_p	$3.8\ kJ/(kg \cdot K)$
Molar enthalpy of CO_2	h_{CO_2}	$94.4 \times 10^3\ kJ/kmol$
Molar enthalpy of MEA	h_{MEA}	$8.2 \times 10^3\ kJ/kmol$

The concentration profile of CO_2 in the liquid film absorbed into aqueous MEA solution is presented in Figure 5-1. Here, MEA concentration was assumed constant in the liquid film. Figure 5-1 showed the comparison of CO_2 concentration of this thesis solved by partial differential equations with boundary conditions (eq 4.16) and that of semester project solved by matrix equations (from eq 4.13 to 4.15).

The interface between the liquid and gas first comes into contract with the CO_2, and the CO_2 concentration in the plane of the interface is uniformly equal to CO_2 equilibrium concentration at interface. This concentration corresponds to the solubility of CO_2 at the partial pressure prevailing above the surface of the liquid, and is assumed to be constant. The CO_2 concentration at interface was calculated according to Henry's law in both project and thesis. In general, the concentration varies with time and with space. However, the concentration was only considered under steady-state condition in both cases. That is to say, time was not been taken into account neither in project nor in thesis. It is further assumed that the diffusion of CO_2 into the liquid does not appreciably affect the temperature or other physical properties of the latter. Due to the chemical reaction between CO_2 and MEA, the reaction rate must to be introduced into the diffusion equations. The reaction rate depends on the local concentration of CO_2 and MEA. Here, the MEA concentration was assumed to remain constant in both cases. The concentration of CO_2 in the liquid bulk was assumed to be 0, since CO_2 loading equalled to 0 in the initial case and CO_2 was completely absorbed by MEA within liquid film. We can conclude from Figure 5-1 that the thesis results solved by partial differential equations accompanied by boundary conditions were perfectly match the project results calculated using matrix equations.

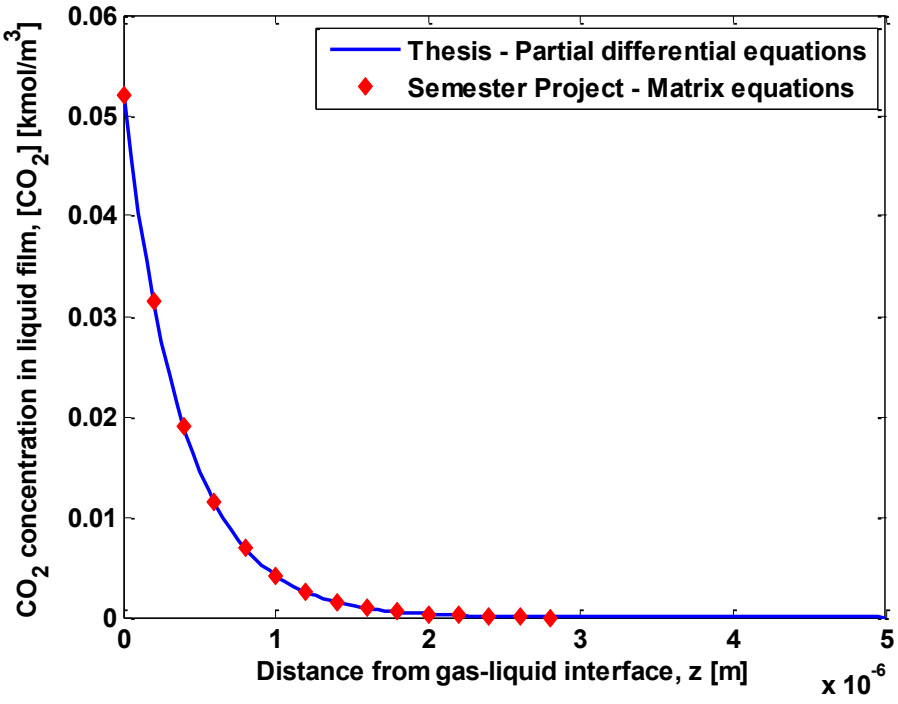

Figure 5-1 Concentration profile of CO_2 in the liquid film absorbed into aqueous MEA solutions

5.2 CO_2 and MEA concentration profile

The concentration profile of CO_2 and MEA in liquid film is presented in Figure 5-2. The concentrations were calculated based on partial differential equations with boundary conditions (eq 4.16 and eq 4.17).

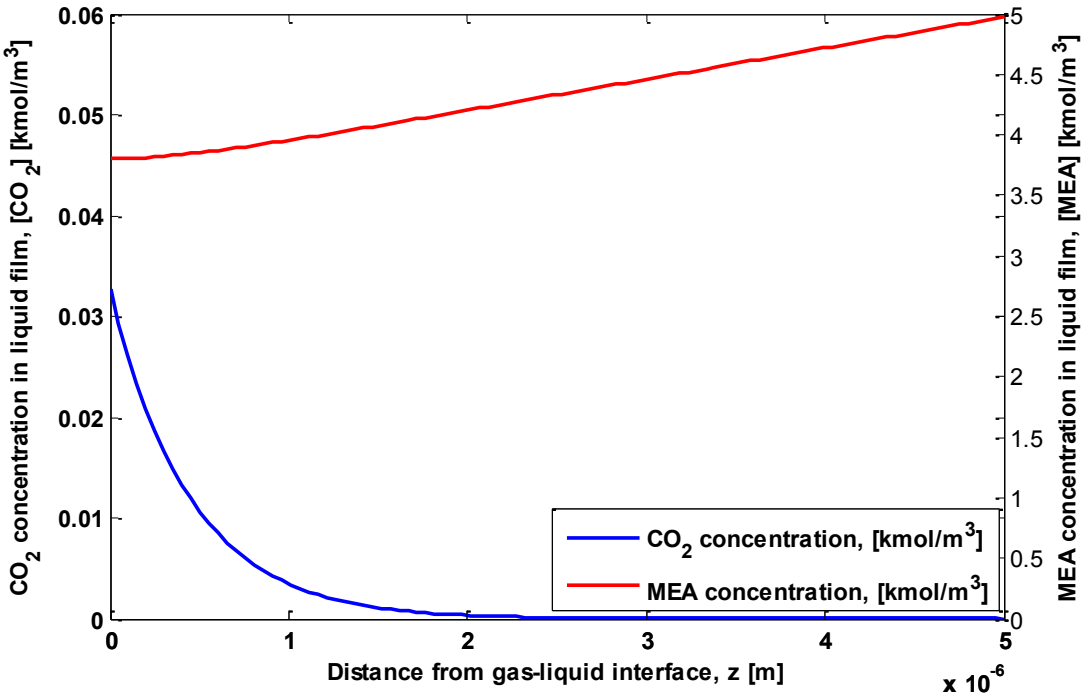

Figure 5-2 Concentration profile of CO_2 and MEA in liquid film

Previous published literatures concluded that zwitterion mechanism could explain the reaction kinetics of the CO_2-MEA very well (Vaidya and Kenig 2007). The reaction is of the first order with respect to both CO_2 and MEA in aqueous system, thereby suggesting that zwitterion deprotonation is instantaneous. The reaction rate is equal to the rate at which CO_2 and MEA can diffuse to the reaction plane. The initial concentration of MEA is uniformly equal to given feeding MEA concentration, and 2 moles of it react with each mole of CO_2 due to stoichiometry. In this thesis work, the reaction was assumed to undergo a pseudo-first order reaction. The rate of reaction at any point is proportional to the local concentrations. Truly first-order irreversible reactions are seldom encountered in practice. However, when the solute gas undergoes a reaction with a dissolved reactant, which is first-order with respect to concentration of dissolved gas, then under certain circumstances, the concentration of the reactant may be almost uniform and the reaction rate of dissolved gas will then be approximately proportional to its local concentration.

Physically, the pseudo-first order means that the MEA diffuses towards the interface fast enough to prevent the reaction causing any significant depletion there. The concentration profile of MEA in Figure 5-2 shows significant depletion of free MEA towards the gas-liquid interface. That indicates that the assumption of pseudo first-order reaction to drive the simplified kinetics models is not accurate because the concentration of the reactive species, here is MEA, is not in a large excess and is not constant throughout the liquid phase. This highlights the importance of applying a numerical model to obtain reaction kinetics from absorption experimental data.

5.3 Estimation of Temperature Gradient in Liquid Film

In the following, the model for the temperature gradient in liquid film has been investigated, as described in chapter 4.4. In the simulation model, the liquid film is further divided into film columns with *dx* width, *1 m* length and *1 m* height. Those columns are assumed as thermal isolated systems. The temperature increase above the bulk phase is only due to heat produced with respect to chemical reaction at local condition, and no heat transfer in and out from neighboring columns.

Figure 5-3 indicates that the reaction heat decreases with distance from gas-liquid interface to liquid bulk phase. According to equation 4,19, the reaction heat only depends on reaction rate calculated by using local CO_2 and MEA concentration in a certain temperature, as the reaction enthalpy and reaction volume are assumed constant in this case. The heat production reaches maximum at the interface where has the highest reaction rate, and agree well with CO_2 concentration profile in the liquid film.

Temperature gradient in liquid column is estimated and the result is presented in Figure 5-4. Temperature gradient has the same trend as reaction heat profile, which decreases with distance from gas-liquid interface. At the interface, temperature is raised approximately 6 K per second in the corresponding thermal isolated liquid column. However, liquid column is impossible to be an adiabatic system in reality, so the reaction heat is conducted to surrounding columns. The heat transfer model with consideration of heat conduction is developed in this thesis, and the model and result are detailed presented in chapter 4.5 and chapter 5.4, respectively. Temperature rises about 0.15 K at interface once heat conduction is taken into account, as shown in Figure 5-5, which is significantly lower than temperature rise in thermal isolation system. This indicates that the heat produced by chemical reaction is conducted fast enough, and temperature does not significantly rise in the liquid film above bulk phase. Therefore, the model without heat conduction consideration estimates the maximum temperature gradient in the liquid film, and it is not very realistic.

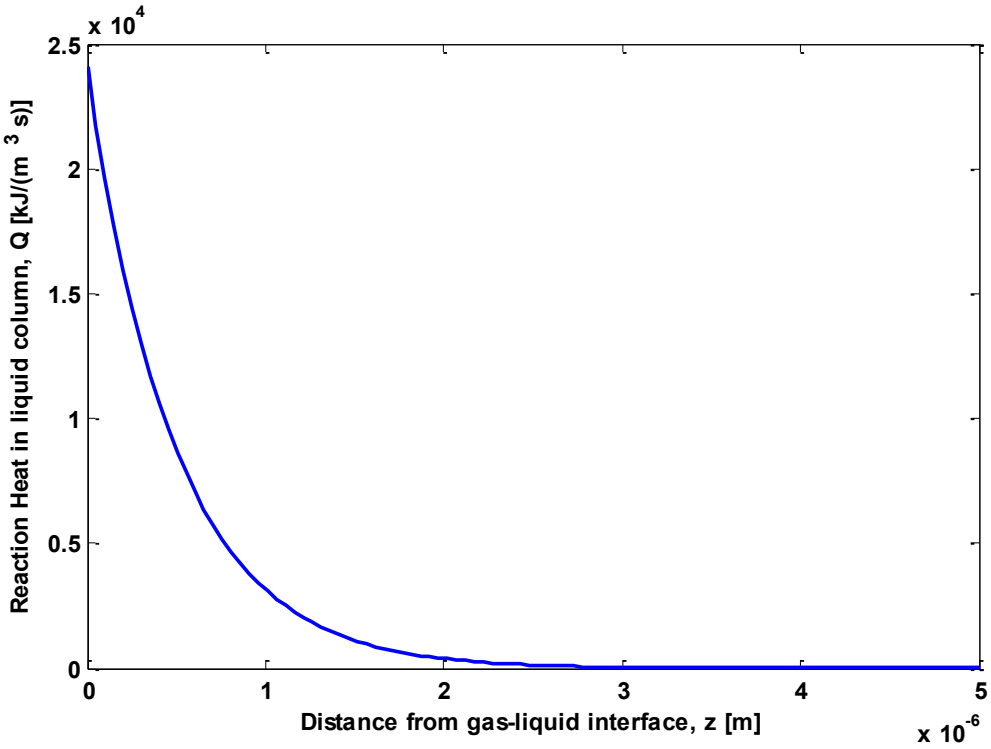

Figure 5-3 Produced heat due to chemical reaction in liquid column

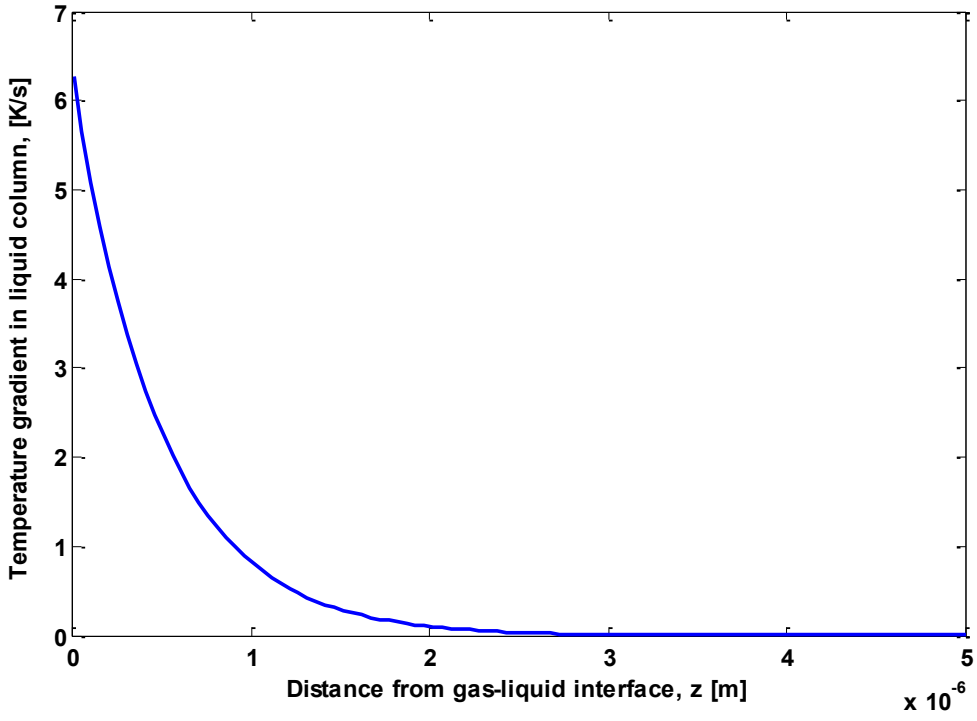

Figure 5-4 Temperature gradient profile in liquid film

5.4 Energy Balance

The temperature profile in liquid film is presented in Figure 5-5 at given initial simulation conditions. The temperatures were calculated based on partial differential mass and heat transfer equations with boundary conditions (eq 4.16, eq 4.17 and eq 4.25).

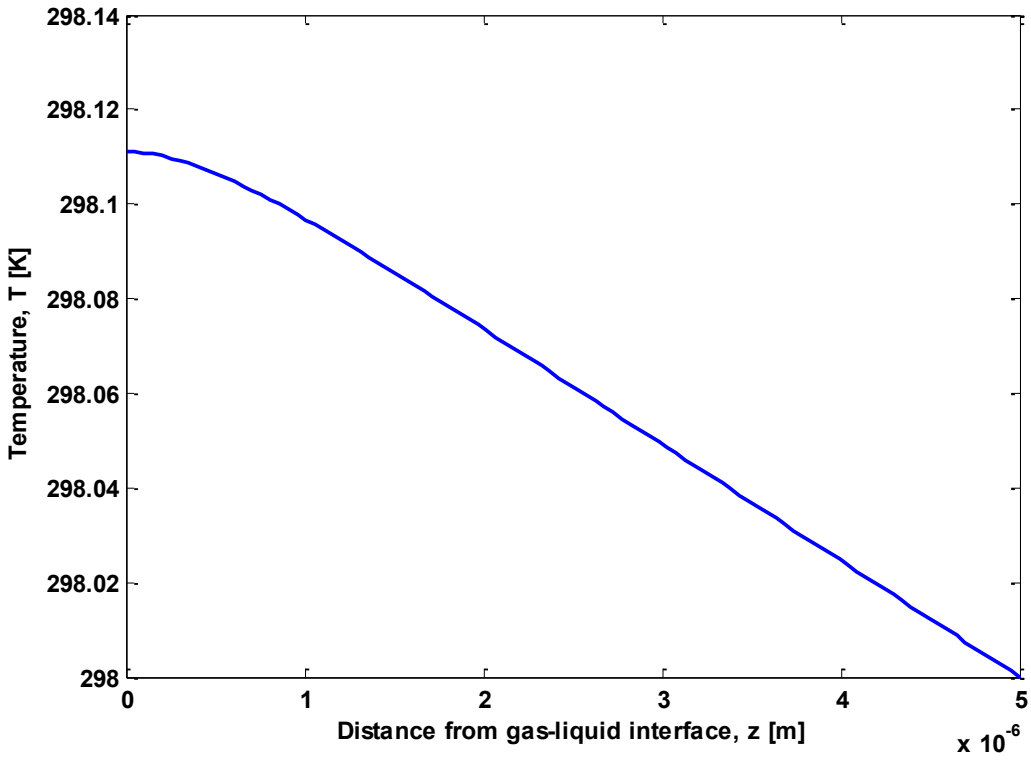

Figure 5-5 Temperature profile in liquid film

When CO_2 diffuses into aqueous MEA solutions, the temperature in the neighbourhood of interface will tend to rise because of the exothermic nature of the physical absorption of the CO_2, and the rise will be enhanced since the CO_2-MEA reaction is exothermic. If the rise in temperature is large enough it will affect the rate of absorption because of its effect on solubility, diffusivity and reaction rate. However, this case was based on the assumption that it was insufficient to affect solubility, diffusivity or reaction rate appreciably. Meanwhile, it was assumed that no heat was transferred from the liquid film to gas film. Such a loss would reduce the rise in temperature at the interface. The simulated temperature-rise is somewhat greater than the actual temperature rise.

The temperature rise consists of two independent terms. The first is the rise due to the heat of absorption, which is liberated in the plane of the interface; the second is due to the

reaction between CO_2 and MEA in the liquid film. The total temperature rise at the interface is the sum of those two independent terms. Under the simulation parameter conditions in this case, where the initial temperature was set as 298 K and film thickness was 5×10^{-6} m, the temperature raised 0.11 K within the interface. Danckwerts (1970) has numerically calculated the temperature rise at interface in various gas absorption circumstances. The rise in temperature at interface for CO_2 absorption by various chemical solutions is in the range from approximately 0.05 to 0.2 K (Danckwer 1970). However, the numerical data particular for CO_2 absorption by MEA was not presented in the book. The interfacial temperature rise simulated in this thesis is in the temperature range presented in the book, although the absorbent solution is different. Hence, the simulation result in this thesis agrees well with previous study, but further experiment and numerical calculation particular for MEA solution is required.

6. Discussion of Sensitivity Analysis

6.1 Effects of Operating Temperature

The effects of operating temperature on CO_2 and MEA concentration in liquid film at 298K, 313K and 333 K are presented in Figure 6-1.The parameter inputs for simulation are given in Table 6-1.

Table 6-1 Parameter inputs for simulation

Parameter	Value
Film thickness	$5 \times 10^{-6}\ m$
Pressure	10 kPa
CO_2 partial pressure, y_{CO_2}	1.0
CO_2 loading, α	0
MEA mass weight, *wt%*	30%

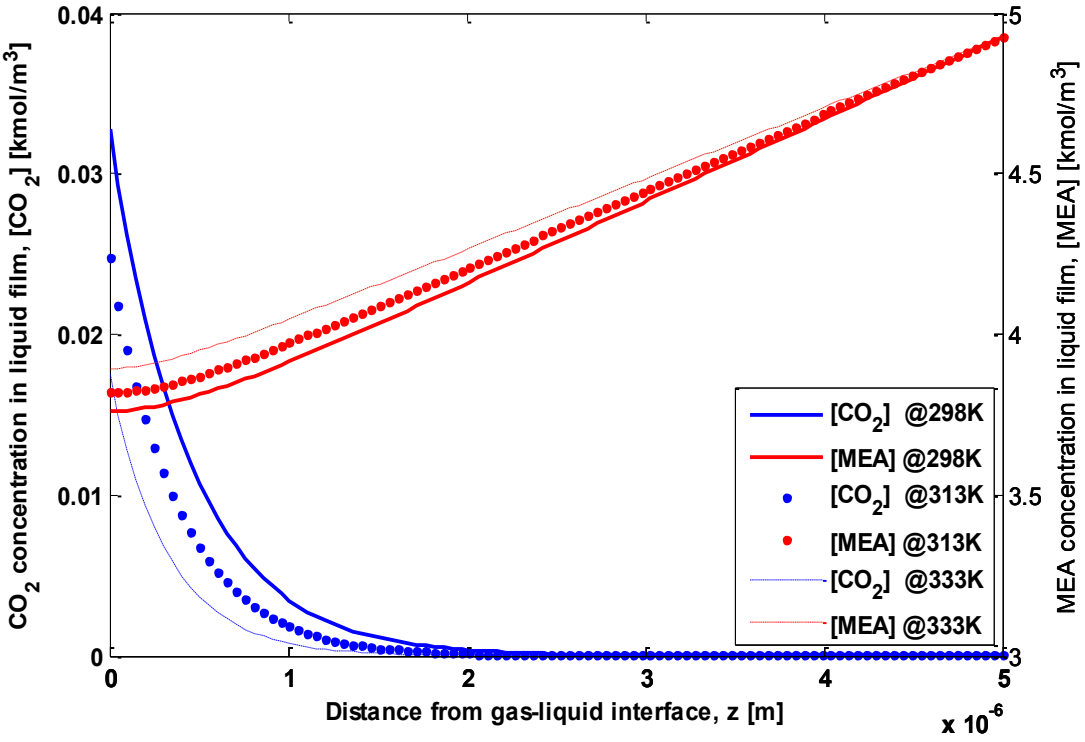

Figure 6-1 Effects of operating temperature on CO_2 and MEA concentration in liquid film

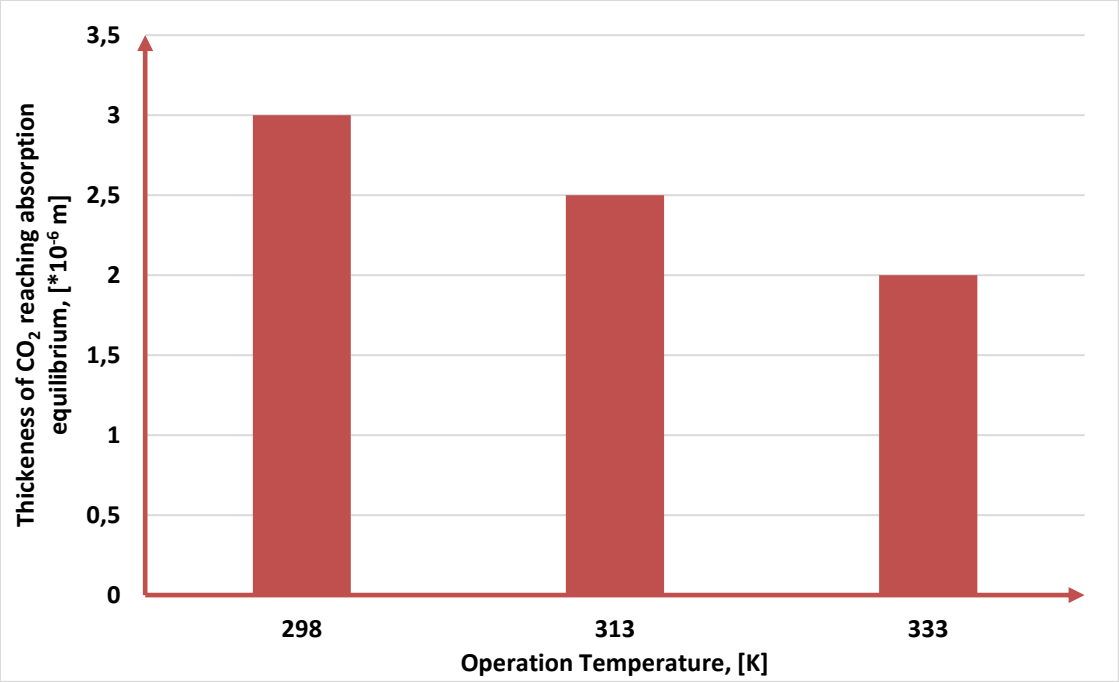

Figure 6-2 Effects of operation temperature on thickness of CO_2 reaching absorption equilibrium

The concentration of CO_2 at interface significantly decreases with increasing operating temperature at a certain concentration, which is approximately 0.33, 0.25 and 0.18 kmol/m^3 at 298 K, 313 K and 333 K operation temperature, respectively. The boundary condition at gas-liquid interface determined by Henry's law equation (eq 4-16 and eq 4-17), shows that CO_2 interfacial concentration is a relation of partial pressure to Henry's constant. In this thesis, Henry's constant of CO_2 in aqueous MEA solution was estimated according to the N_2O analogy method, and the data on the physical solubility of absorbed gas (N_2O and CO_2) in various MEA are dependent of temperature. A semi-empirical model proposed by Penttila et at (Penttila, Dell'Era et al. 2011) has been used here, which fits the experimental data. Henry's constant of CO_2 in aqueous MEA solutions increases systematically with increasing temperature at a certain MEA concentration, which was concluded by Ying et al (Ying, Eimer et al. 2012).

The concentration profile also indicates the penetration depth of diffused CO_2 into the liquid. Figure 6-2 shows the effects of operation temperature on thickness of CO_2 reaching absorption equilibrium. The depth of equilibrium decreases with increasing temperature. The absorption flux of CO_2 rises with increasing operation temperature due to higher diffusivity coefficient and reaction rate. As a result, the absorption equilibrium can be achieved within shorter thickness at higher temperature condition.

The concentration profiles of CO_2 and MEA are affected by the chemical absorption rate and diffusion (Aboudheir 2003). We can see from Figure 6-1 that the depletion of free MEA towards the gas-liquid interface decreases with increasing temperature. The diffusivity of MEA is increasingly with operation temperature (Littel, Versteeg et al. 1992). Physically, this means that MEA diffuses towards the gas-liquid interface fast to eliminate the reaction causing any significant depletion (Danckwer 1970).

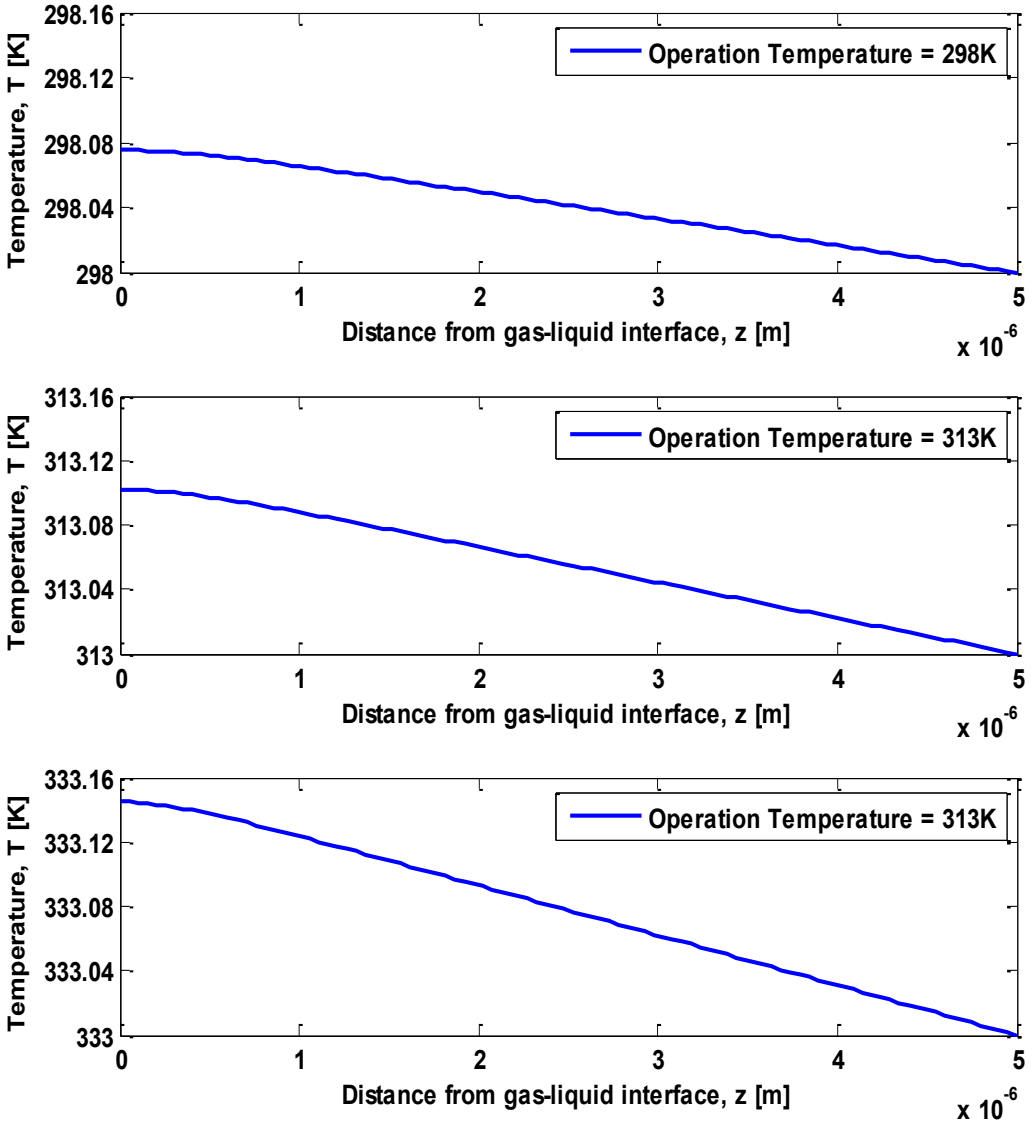

Figure 6-3 Effects of operating temperature on temperature profile in liquid film

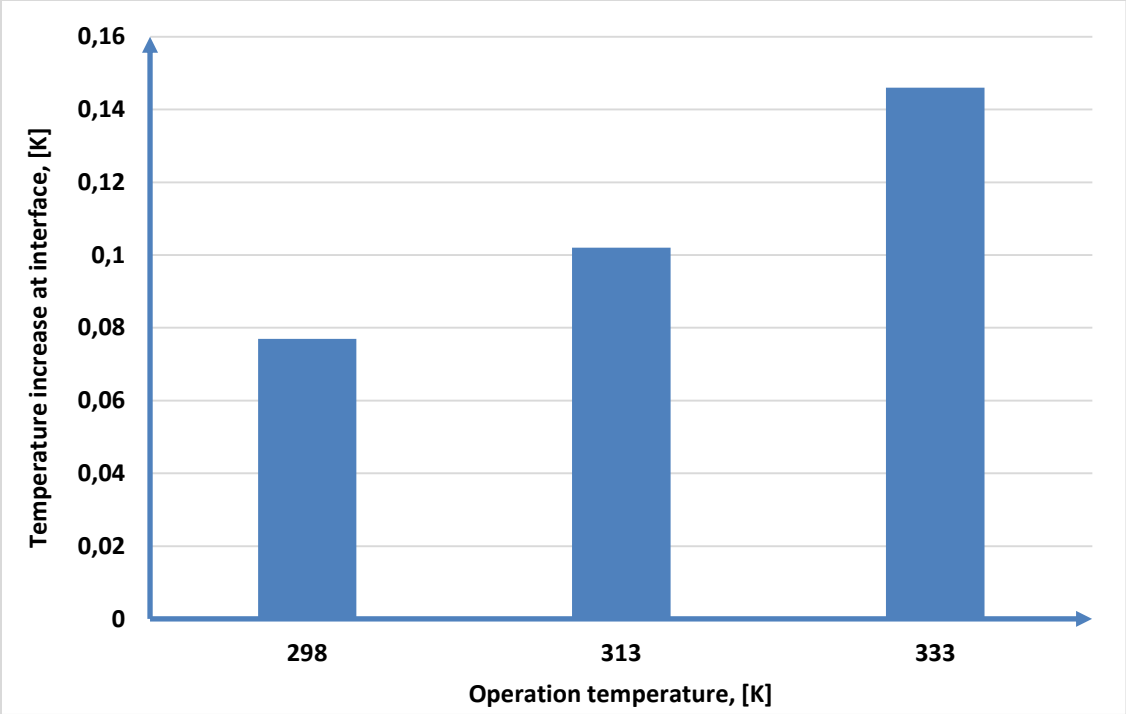

Figure 6-4 Effects of operation temperature on temperature increase at interface

The effects of operating temperature on the temperature profile within the liquid film are presented in Figure 6-3, and the temperature-rise at interface is shown in Figure 6-4. We can see from those two figures that the temperature at interface is not raised significantly above the bulk temperature by the absorption and reaction processes. The simulated rises in temperature are approximately 0.08 K, 0.11 K and 0.15 K at 298 K, 313 K and 333 K operating temperature, respectively. Those are in agreement with numerical calculation presented in book *Gas-Liquid Reaction* (Danckwer 1970). The rise in temperature is the sum of two terms – that due to the heat of physical absorption, which is liberated at the interface; and that due to the heat of reaction, which is liberated in the liquid film for the film model. The rate of physical absorption increases with the operating temperature because of the increasing of Henry's constant of CO_2 in aqueous MEA solutions, as well as the increasing of chemical reaction rate results in temperature rise.

6.2 Effects of CO_2 Loading

The concentration profiles of CO_2 and MEA in the liquid film with various CO_2 loading aqueous MEA solutions (0, 0.2 and 0.4 mol/mol) are presented in Figure 6-5. The simulation parameters are shown in Table 6-2.

Table 6-2 Parameter inputs for simulation

Parameter	Value
Film thickness	$5 \times 10^{-6}\ m$
Temperature	298 K
Pressure	10 kPa
CO_2 partial pressure, y_{CO_2}	1.0
MEA mass fraction, *wt%*	30%

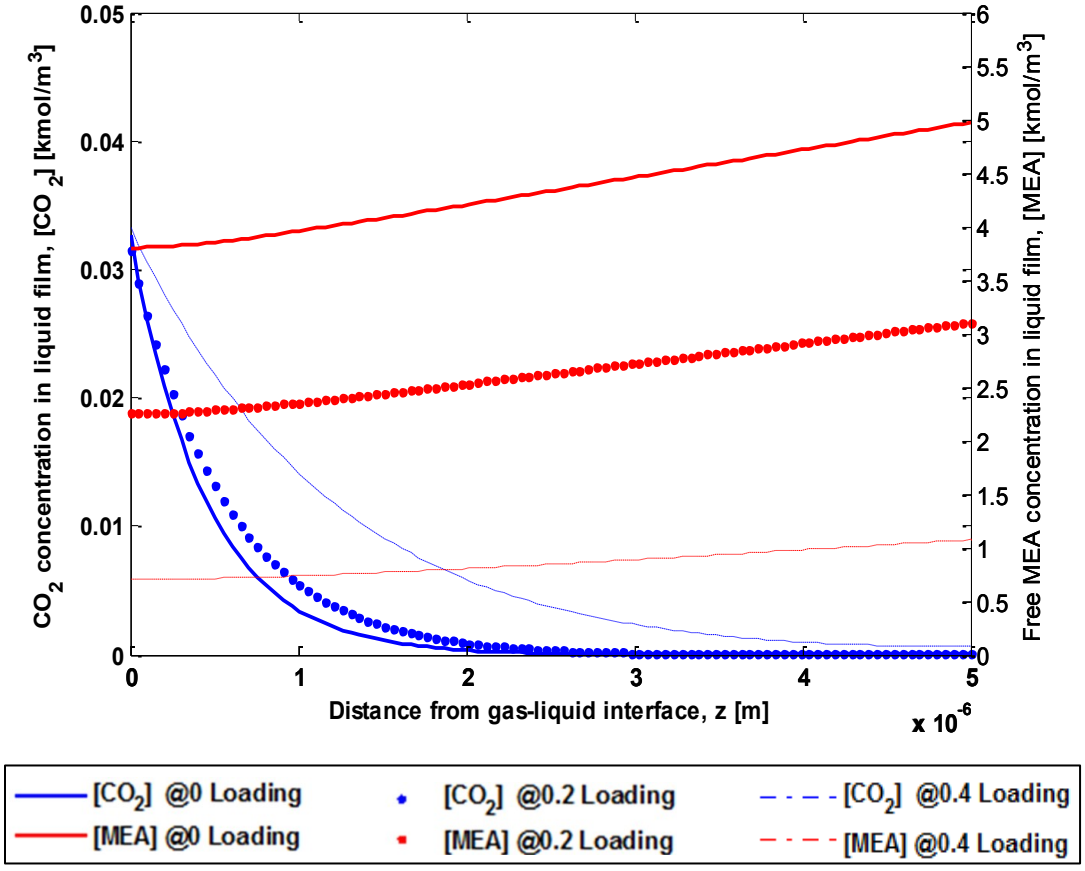

Figure 6-5 Effects of CO_2 loading on CO_2 and MEA concentration in liquid film

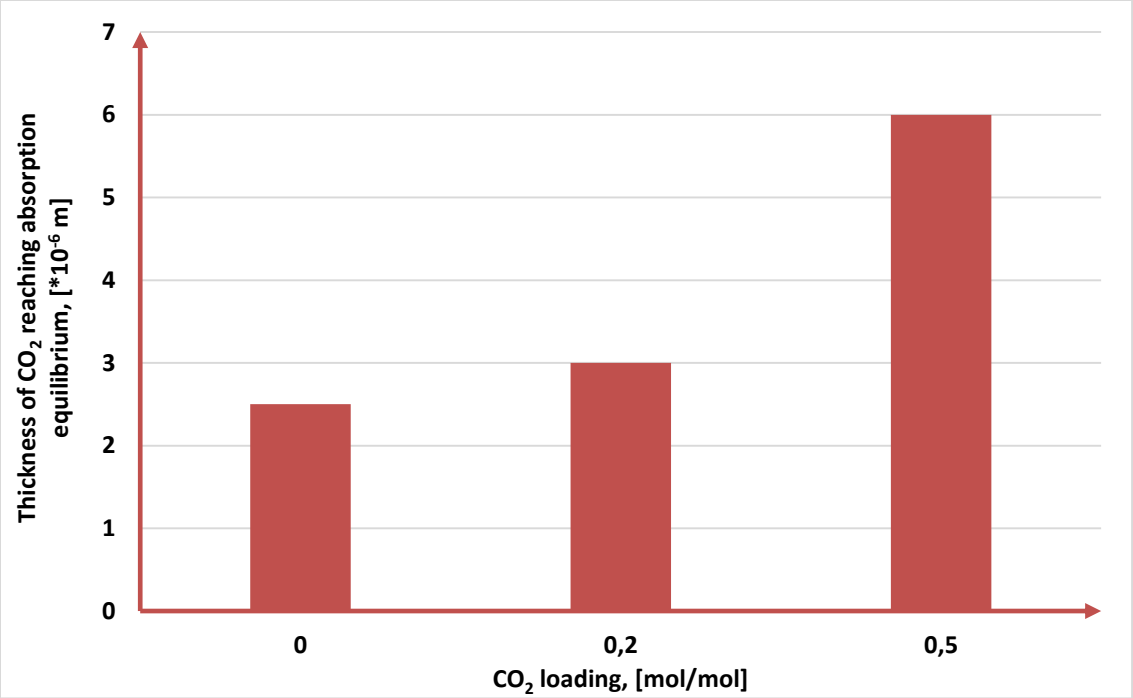

Figure 6-6 Effects of CO_2 loading on liquid film thickness

CO_2 loading does not significantly affect the concentration of CO_2 at interface. As presented above, the interfacial CO_2 concentration changes due to Henry's constant. Browning and Weiland presented that except temperature both amine concentration and CO_2 loading affect the solubility of CO_2 (Browning and Weiland 1994). In addition, the slight increasing of density of aqueous MEA solution with CO_2 loading raises MEA concentration (Weiland, Dingman et al. 1998). However, neither CO_2 loading nor MEA concentration does not significantly increase the Henry's constant of CO_2. As a result, the effect of CO_2 loading on interfacial CO_2 concentration is too small to be taken into account.

The free MEA concentration decreases with CO_2 loading, as presented in concentration profile (Figure 6-5). The depletion of free MEA towards the gas-liquid interface decreases and the diffusivity of MEA increases with CO_2 loading. According to equation 4.5, the diffusivity of MEA is dependent of temperature and free MEA concentration. In this case, with increasing of CO_2 loading, the lower free MEA concentration leads to the higher diffusion of MEA. Therefore, the system experiences less diffusion resistance at higher CO_2 loading due to the inability of depleted reactants to diffuse quickly to the interface. This is in agreement with model data developed by Ross and Gary (Ross 2011).

Figure 6-6 shows the thickness of CO_2 reaching absorption equilibrium increases with CO_2 loading in the initial MEA solution. The chemical reaction rate is slow under high CO_2 loading condition because of low free MEA concentration. Additionally, the diffusion coefficient of CO_2 decreases with CO_2 loading according to equation (4.1) – (4.4). Those two factors contribute the decreasing of CO_2 absorption flux, which consequently lead to longer distance to reach absorption equilibrium. In another word, MEA solution that contains more initial CO_2, takes longer time to absorb CO_2 from gas stream completely.

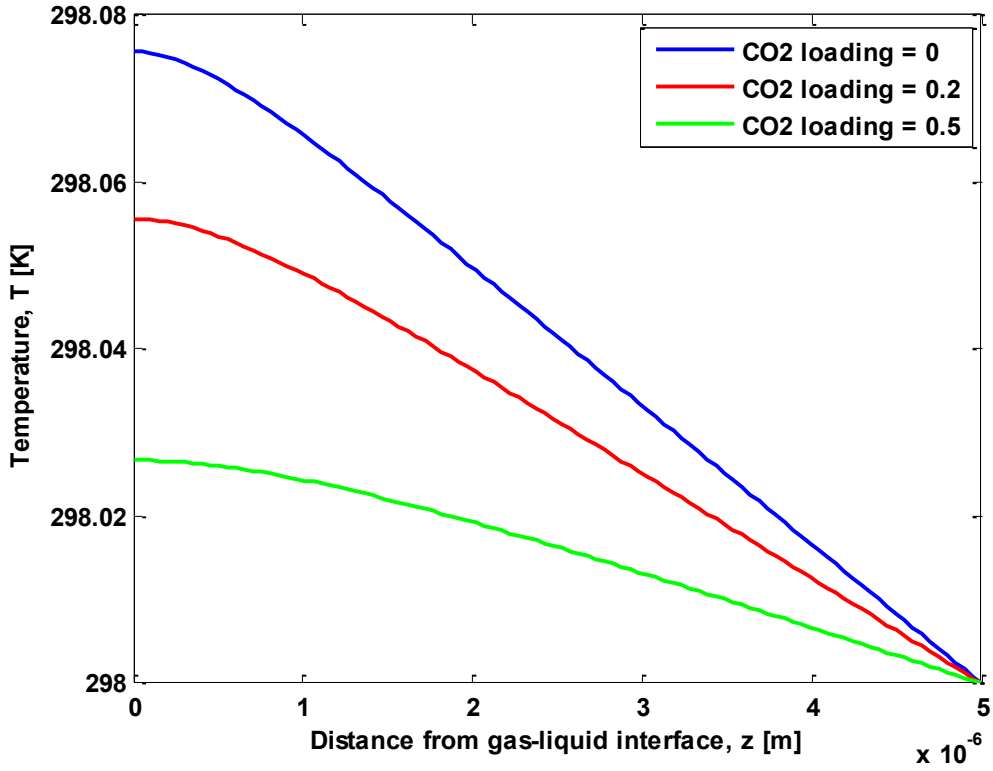

Figure 6-7 Effects of CO_2 loading on temperature profile in liquid film

The effects of CO_2 loading on the temperature profile within the liquid film are presented in Figure 6-7, and the temperature-rise at interface is shown in Figure 6-8. We can see from those two figures that the temperature at interface is not raised significantly above the bulk temperature by the absorption and reaction processes, which agrees with numerical calculation presented in book *Gas-Liquid Reaction* (Danckwer 1970). The simulated interfacial temperature-rise were approximately 0.074 K, 0.056 K and 0.028 K at 0, 0.2 and 0.4 CO_2 loading, respectively. As presented above, the effect of heat of physical absorption can be ignored since the Henry's constant of CO_2 does not increase significantly with CO_2 loading, whereas this decreases the reaction rate. Moreover, the

heat conductivity of aqueous MEA solution decreases with increasing of CO_2 loading. To conclude that higher CO_2 loading raise less temperature at interface.

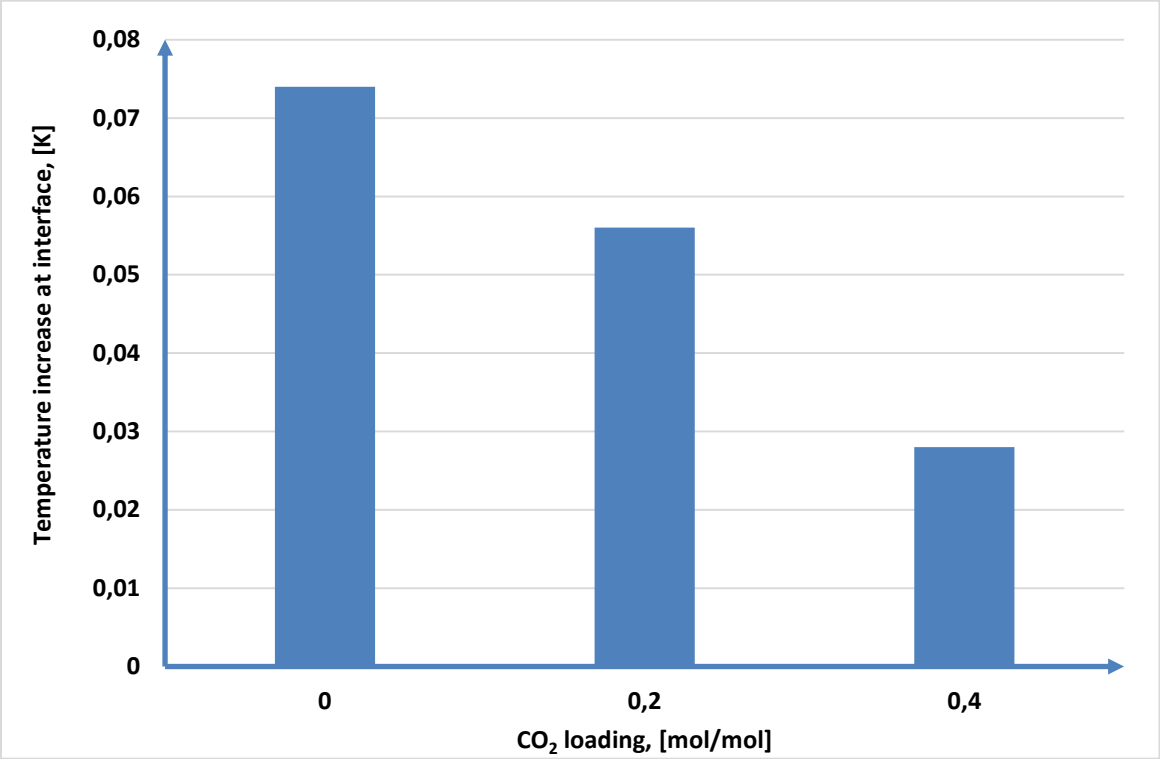

Figure 6-8 Effects of CO_2 loading on temperature increase at interface

6.3 Effects of Initial MEA Mass weight

The simulation results with varying MEA mass weight in the concentration profile of CO_2 and MEA in the liquid film are presented in Figure 6-9. The simulation parameters are given in Table 6-3.

Table 6-3 Parameter inputs for simulation

Parameter	Value
Film thickness	$5 \times 10^{-6}\ m$
Temperature	298 K
Pressure	10 kPa
CO_2 partial pressure, y_{CO_2}	1.0
CO_2 loading, α	0

Figure 6-9 shows that MEA mass weight does not significantly affect CO_2 concentration at interface. As presented above, the concentration of CO_2 at interface is related with Henry's constant. Experimental data measured by Ying shows that the Henry's constant of CO_2 in MEA solution is not significantly affected by MEA concentration in the low concentration range (from 10 wt% to 30 wt%) (Ying, Eimer et al. 2012). The sensitivity analysis was simulated within this range in the thesis. It can also be explained by the influence trends of MEA concentration on density of aqueous MEA solution (Amundsen, Oi et al. 2009). The difference of densities of non-CO_2 preloaded MEA solution among 10 wt%, 20 wt% and 30 wt% are not significant, which are 1002, 1007 and 1013 kg/m^3, respectively (Weiland, Dingman et al. 1998). Therefore, MEA mass weight does not significantly affect CO_2 concentration at interface.

To complete CO_2 absorption in the liquid film requires longer distance at lower MEA mass %, as presented in Figure 6-9 and Figure 6-10. The thicknesses of CO_2 reaching absorption equilibrium are 4.4×10^{-6}, 3×10^{-6} and 2.3×10^{-6} m at 10 wt%, 20 wt% and 30 wt%, respectively. Since pseudo-first order reaction has been assumed in this thesis, the reaction rate is proportional to the concentration of CO_2 and MEA. Obviously, it is slow at low initial MEA concentration.

Figure 6-9 also shows that the depletion of MEA towards the gas-liquid interface increases with MEA mass weight, which is due to decreasing of MEA diffusivity coefficient. It is opposite from the effect trend of CO_2 loading. Therefore, the depletion of MEA to interface is due to reaction rate.

Figure 6-11 shows the simulation result of temperature profile in the liquid film. The MEA concentration of 10 wt%, 20 wt% and 30 wt% are investigated. The temperature at interface is not raised significantly above the bulk temperature by the absorption and reaction processes. The rise-temperature at interface increases with MEA mass %, as presented in Figure 6-12. The simulated results were approximately 0.04, 0.062 and 0.075 at 10 wt%, 20 wt% and 30 wt%, respectively. As presented before, the contribution from physical absorption can be ignored since the Henry's constant does not increase significantly with MEA mass %, whereas the chemical reaction dominates the temperature rise at interface. The system increase higher temperature at interface under higher MEA mass % condition, which is due to higher reaction rate.

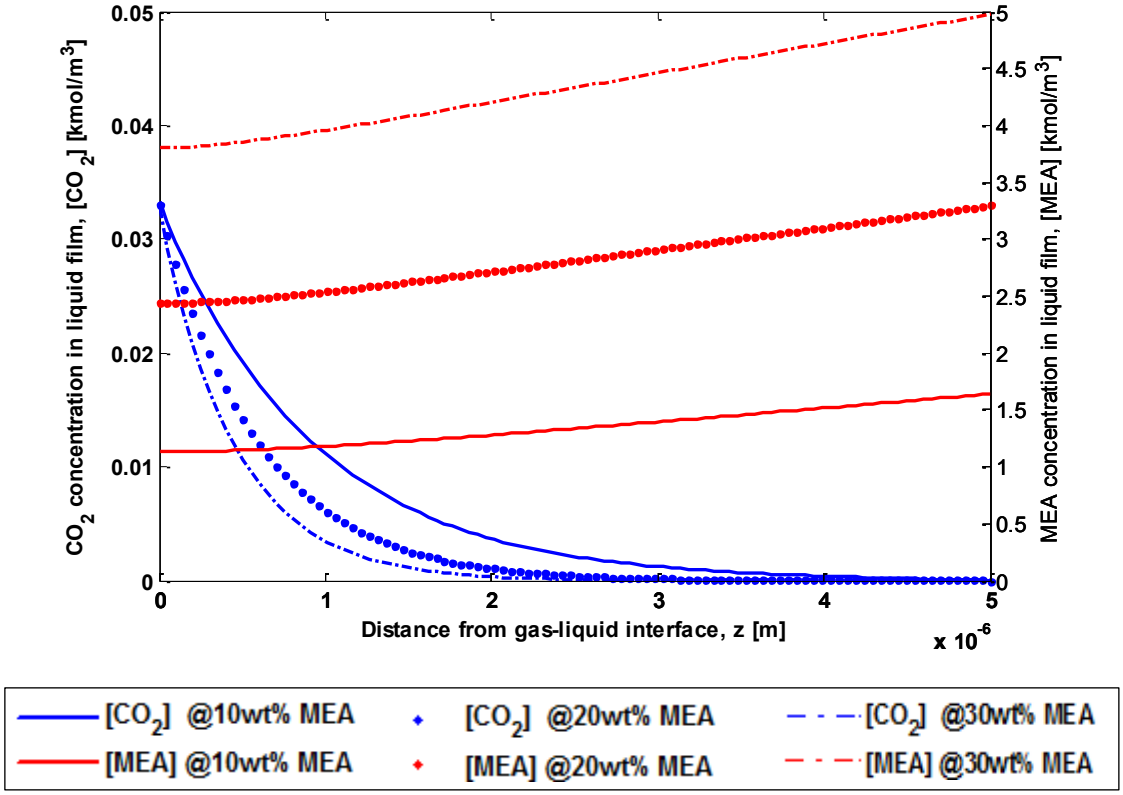

Figure 6-9 Effects of initial MEA mass weight on CO_2 and MEA concentration in liquid film

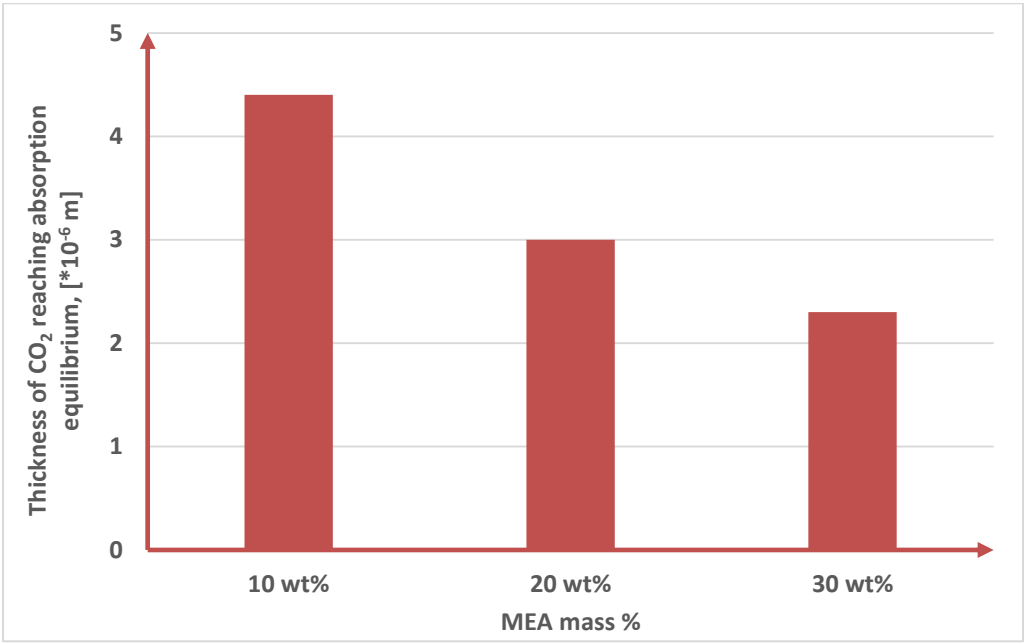

Figure 6-10 Effects of MEA mass weight on thickness of CO_2 reaching absorption equilibrium

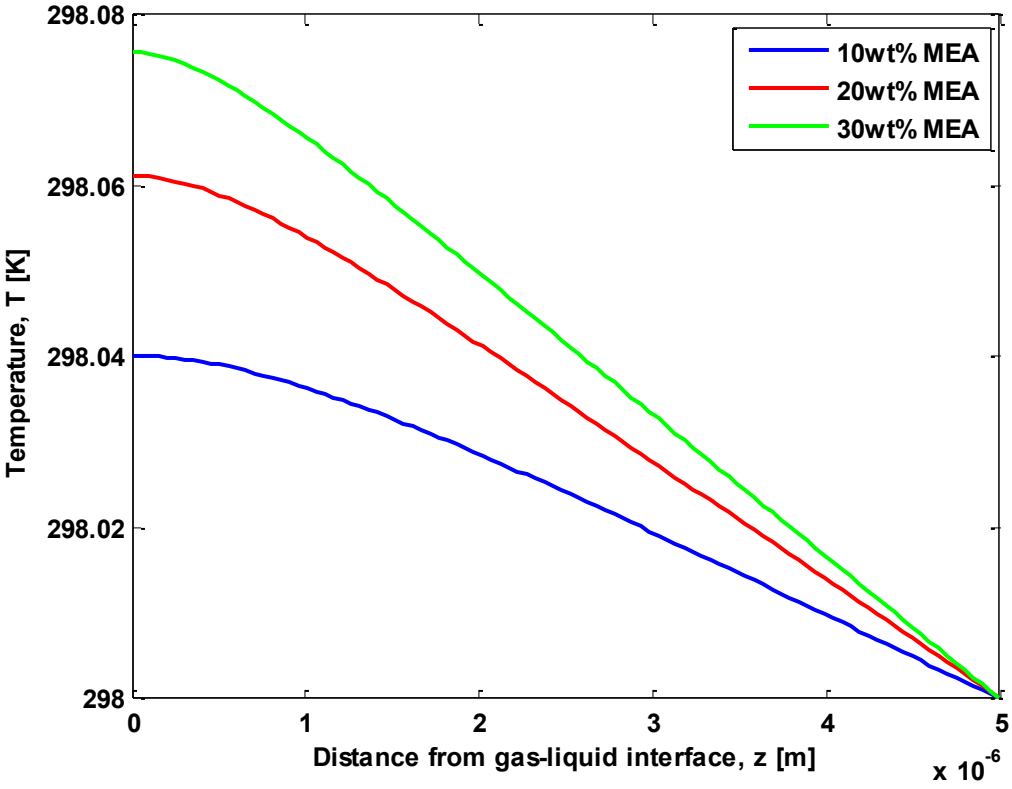

Figure 6-11 Effects of initial MEA mass weight on temperature profile in liquid film

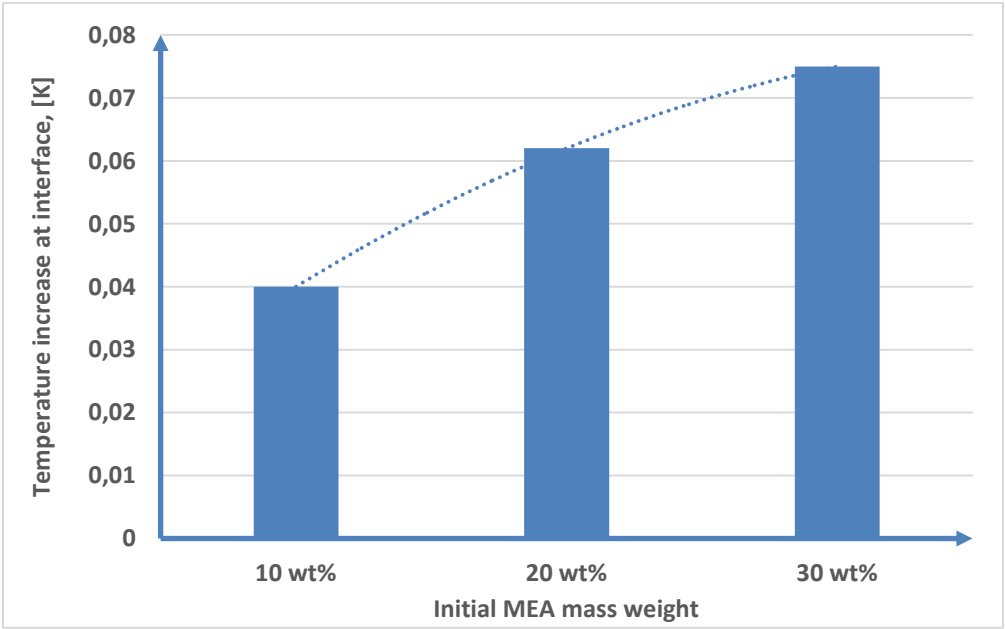

Figure 6-12 Effects of initial MEA mass weight on temperature increase at interface

6.4 Temperature Rise at Interface

The comparison of temperature rise at interface is investigated by matrix cases study in this thesis. The results are presented from Figure 6-13 to Figure 6-18. Those figures imply that the temperature at the surface of the MEA is raised from approximately 0.1 to 0.16 K in various circumstances, ant it is not raised significantly above the bulk temperature in those cases due to physical absorption and chemical reaction processes. Danckwerts (1970) has numerically calculated the temperature rise at interface in various gas absorption circumstances. The rise in temperature at interface for CO_2 absorption by various chemical solutions is in the range from approximately 0.05 to 0.2 K (Danckwer 1970). However, the numerical data particular for CO_2 absorption by MEA was not presented in the book. The interfacial temperature rises simulated in this thesis are in the temperature range presented in the book, although the absorbent solution is different. Hence, the simulation result in this thesis agrees well with previous study, but further experiment and numerical calculation particular for MEA solution is required. According to simulation results expressed in Figure 6-13 and Figure 6-17, under the same CO_2 loading or MEA mass weight (wt%) system, with the increase in operation temperature the temperature rise at interface increases accordingly. Figure 6-14 and Figure 6-16 show that interfacial rise-temperature increases with MEA mass weight (wt%) under the same CO_2 loading or operation temperature. The temperature rise at interface decreases with increasing of CO_2 loading, under the same operation temperature or MEA mass %, as presented in Figure 6-15 and Figure 6-18. The explanations for temperature rise trend have been presented above individually (chapter 6.1 to chapter 6.3). To sum up, the rise in temperature at the interface is insufficient to affect solubility, diffusivity, and reaction rate. In this thesis, it is assumed that no heat is lost from the liquid to the gas at interface. Any such losses would reduce the actual temperature-rise below the simulation value. Therefore, the effect of temperature rise on system physic-chemical properties can be ignored.

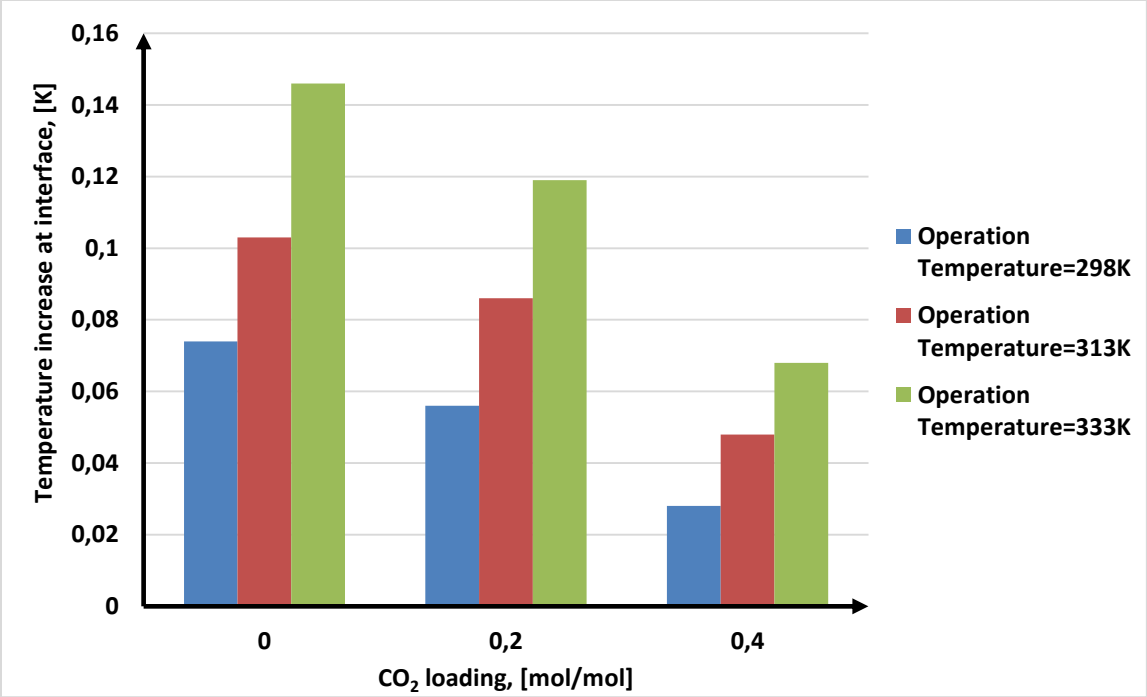

Figure 6-13 Comparison of temperature rise at interface under different CO_2 loading and operation temperature

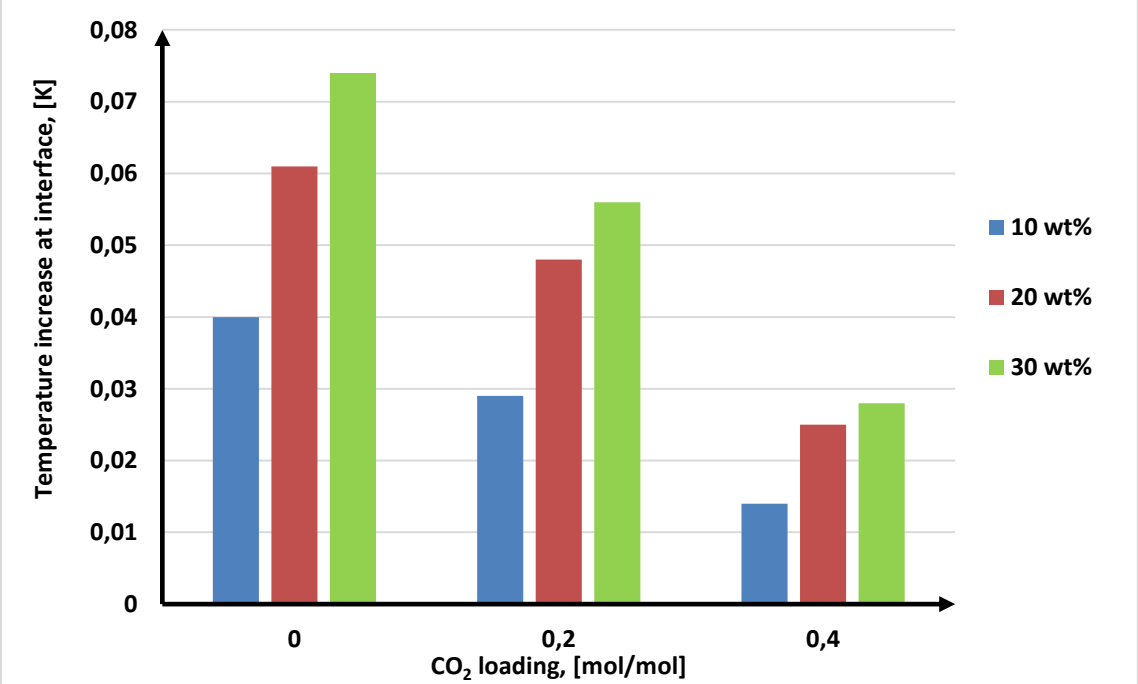

Figure 6-14 Comparison of temperature rise at interface under different CO_2 loading and MEA mass %

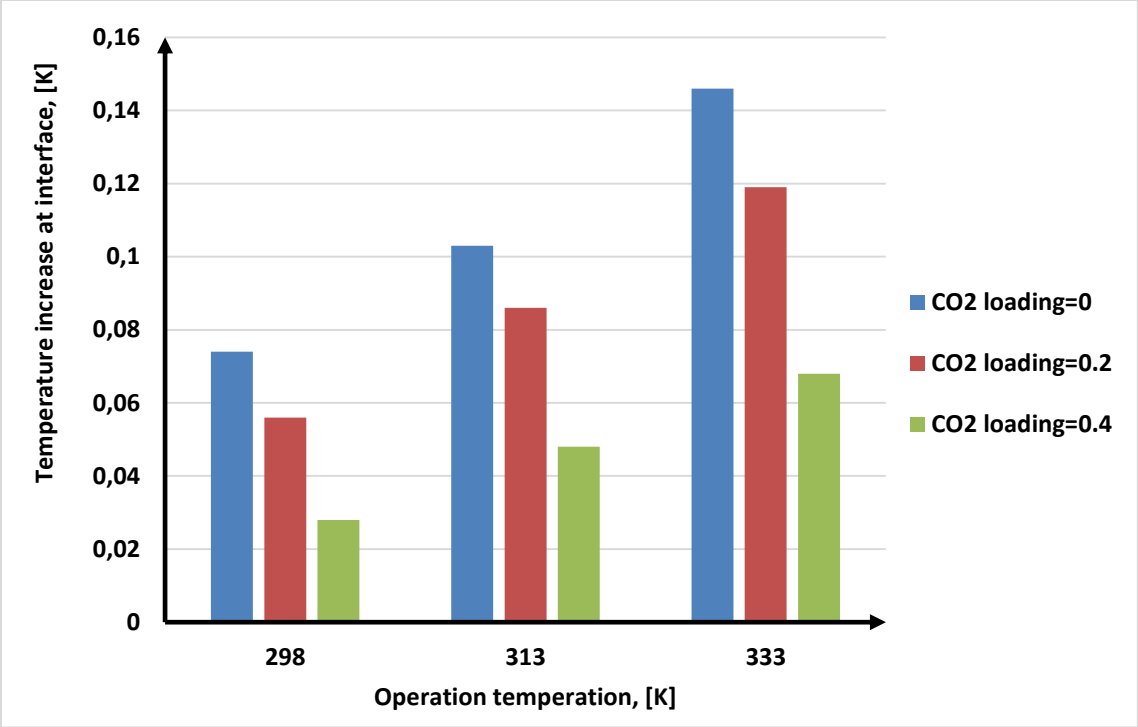

Figure 6-15 Comparison of temperature rise at interface under different operation temperature and CO_2 loading

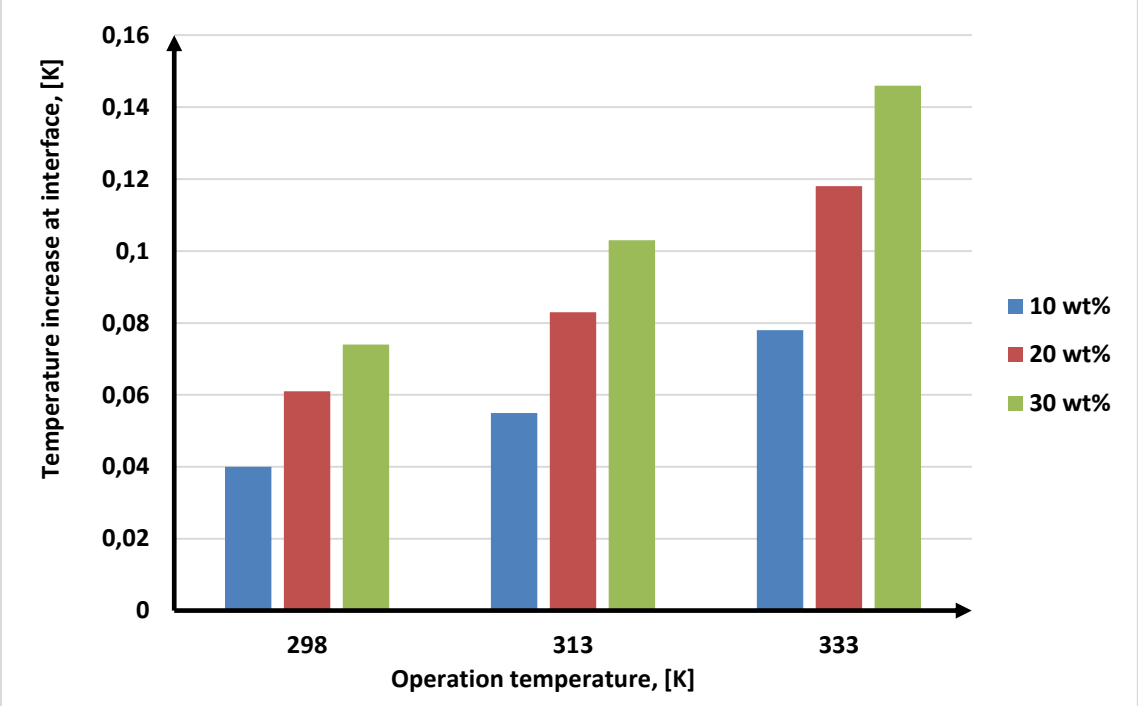

Figure 6-16 Comparison of temperature rise at interface under different operation temperature and MEA mass %

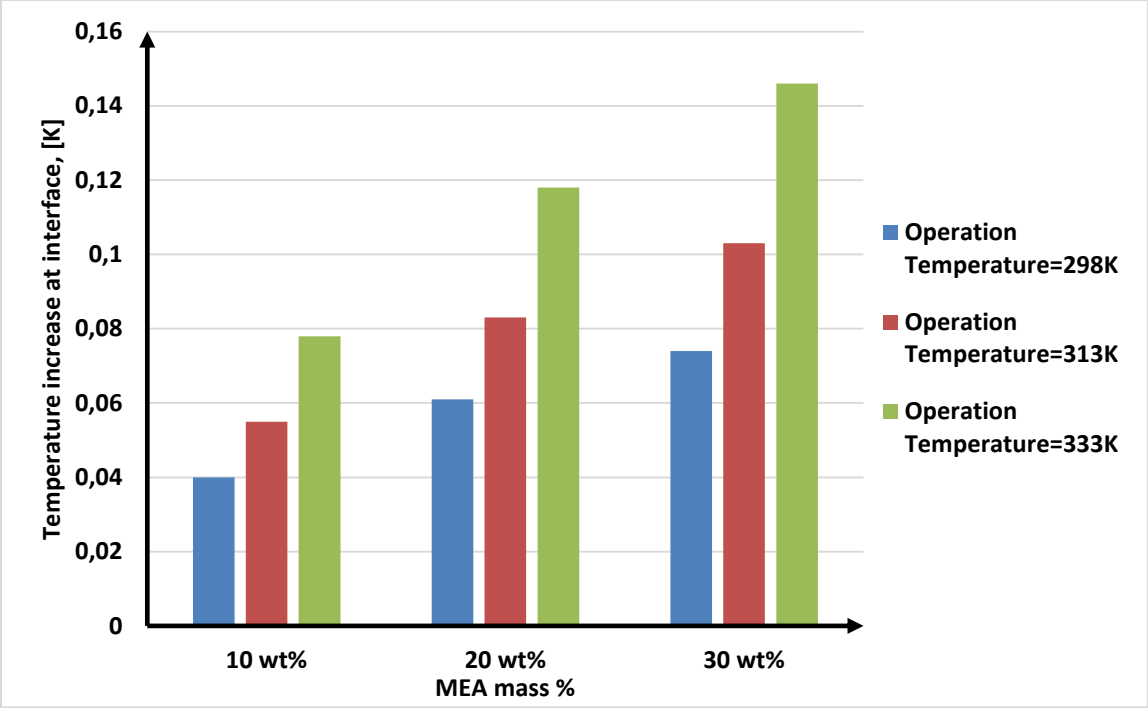

Figure 6-17 Comparison of temperature rise at interface under different MEA mass % and operation temperature

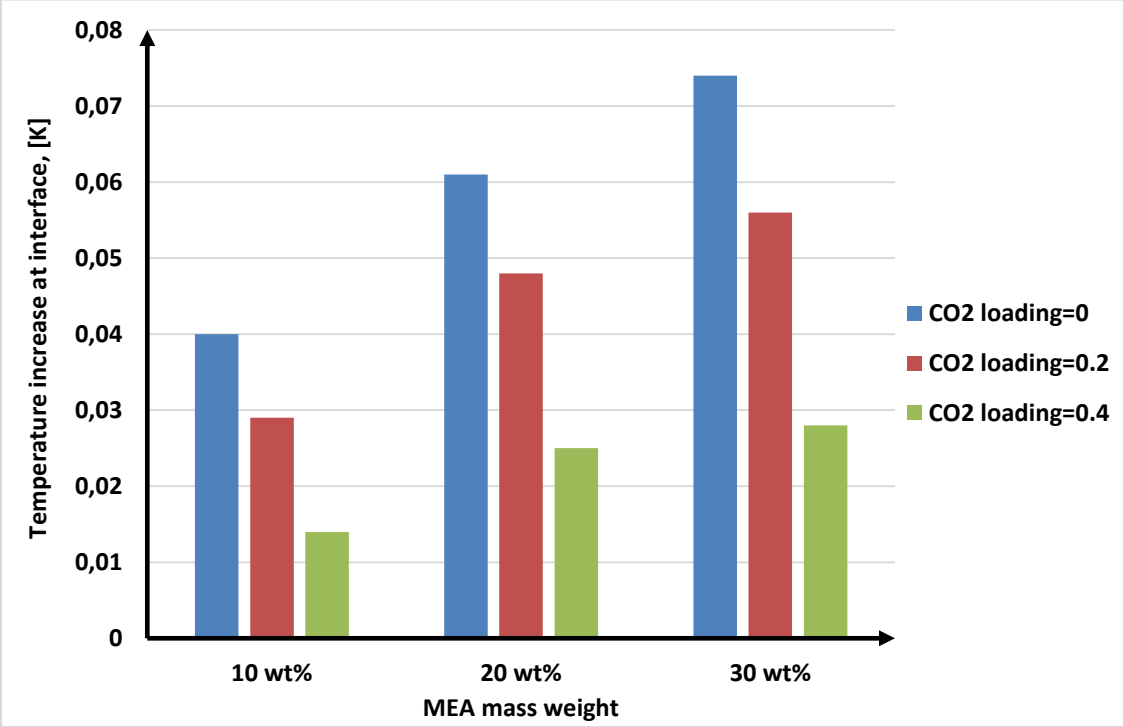

Figure 6-18 Comparison of temperature rise at interface under different MEA mass % and CO_2 loading

7 Conclusion

A rate-based model for CO_2 chemical absorption by MEA is developed. The rate-based model is presented based on two-film model that incorporates mass and heat transference to deal with CO_2-MEA chemical reactions. The model is implemented in MATLAB. The capability of the model to describe the mass and heat transfer has been discussed.

This mass transfer model has shown very good agreement with analytical literature results and with numerical simulation model developed during semester project.

The reaction heat and temperature gradient have been estimated. Both have the same trend as CO_2 concentration, which decrease with distance from gas-liquid interface. The maximum temperature gradient is approximately 6 K/s, and takes place at interface.

Heat transfer model estimates the temperature profile in the liquid film during CO_2 absorption by MEA. The temperature rise is due to physical absorption and exothermic chemical reaction. The rises in temperature at interface in various absorption circumstances are in the range from approximately 0.01 K to 0.16 K, which agree well with numerical calculation done in previous studies. The simulated results by heat transfer model are significantly lower than the rise-temperature simulated by temperature gradient model. This concludes that adiabatic assumption in temperature gradient model is not very realistic, as the heat produced by chemical reaction is conducted fast enough. Hence, heat conduction is necessarily to be considered in energy balance model. Furthermore, the temperature at interface is not raised significantly above the bulk temperature to affect solubility, diffusivity, reaction rate, etc. Therefore, the effect of temperature rise on system physic-chemical properties can be ignored.

The effects of operation temperature, CO_2 loading and initial MEA mass weight (wt%) on the concentration profile and temperature profile in the liquid film have been analyzed. The trend of distance when CO_2 reaches absorption equilibrium is opposite as the trend of temperature rise at interface.

8 Future Work

In future work it is proposed to consider the effect of CO_2-MEA equilibrium in the liquid bulk. In this thesis, the model was established based on the assumption of non-electrolytes solution. Indeed, the thermodynamic properties of electrolyte solutions are distinctive from non-electrolyte solution, including the presence of strong interactions between ions in solutions and the transfer of electrons.

The composition of gas stream was assumed to be pure CO_2 in this thesis. In reality, CO_2 partial pressure at the interface is different from CO_2 partial pressure in gas bulk stream. In order to get precise boundary condition for multi-components initial gas stream, gas film mass transfer coefficient is preferred to be considered in future model development.

It is proposed to develop mass and heat transfer model for the reactive column, and further consider the profile of concentration, the profile of temperature, the profile of the effective mass-transfer area, the pressure drop and etc., over the height of column,

It is recommended in the future work to consider other types of alkanolamine solutions, for example activated MDEA (eg. Piperazine).

References

Aboudheir, A., et al. (2003). "Kinetics of the reactive absorption of carbon dioxide in high CO2-loaded, concentrated aqueous monoethanolamine solutions." Chemical Engineering Science **58**(23-24): 5195-5210.

Aboudheir, A., Tontiwachwuthikul, P., Chakma, A., Idem, R., (2003). "On the Numerical Modeling of Gas Absorption into Reactive Liquids in a Laminar Jet Absorber." The Canadian Journal of Chemical Engineering **81**: 604 - 612

Amundsen, T. G., et al. (2009). "Density and Viscosity of Monoethanolamine plus Water plus Carbon Dioxide from (25 to 80) degrees C." Journal of Chemical and Engineering Data **54**(11): 3096-3100.

Arcis, H., et al. (2011). "Enthalpy of Solution of Carbon Dioxide in Aqueous Solutions of Monoethanolamine at Temperatures of 322.5 K and 372.9 K and Pressures up to 5 MPa." Journal of Chemical and Engineering Data **56**(8): 3351-3362.

Asprion, N. (2006). "Nonequilibrium rate-based simulation of reactive systems: Simulation model, heat transfer, and influence of film discretization." Industrial & Engineering Chemistry Research **45**(6): 2054-2069.

Astarita, G., Savage, D. W., Bisio, A. (1983). Gas treating with chemical solvent. New York, John Wiley.

Baur, R., et al. (2000). "Comparison of equilibrium stage and nonequilibrium stage models for reactive distillation." Chemical Engineering Journal **76**(1): 33-47.

Bird, R. B., Stewart, W. E., Lightfoot, E. N. (1960). Transport Phenomenar. New York, John Wiley & Sons.

Bishnoi, S. and G. T. Rochelle (2000). "Absorption of carbon dioxide into aqueous piperazine: reaction kinetics, mass transfer and solubility." Chemical Engineering Science **55**(22): 5531-5543.

Browning, G. J. and R. H. Weiland (1994). "Physical Solubility of Carbon-Dioxide in Aqueous Alkanolamines Via Nitrous-Oxide Analogy." Journal of Chemical and Engineering Data **39**(4): 817-822.

Campbell, J. M. (1992). Gas Conditioning and Processing.

Caplow, M. (1968). "Kinetics of Carbamate Formation and Breakdown." Journal of the American Chemical Society **90**(24): 6795-&.

Clarke, J. K. A. (1964). "Kinetics of Absorption of Carbon Dioxide in Monoethanolamine Solutions at Short Contact Times." Industrial & Engineering Chemistry Fundamentals **3**(3): 239-&.

Crooks, J. E. and J. P. Donnellan (1989). "Kinetics and Mechanism of the Reaction between Carbon-Dioxide and Amines in Aqueous-Solution." Journal of the Chemical Society-Perkin Transactions 2(4): 331-333.

Danckwer, P. V. (1970). Gas-Liquid Reaction. Great Britain, McGraw-Hill, Inc.

Danckwerts, P. V. (1951). "Significance of Liquid-Film Coefficients in Gas Absorption." Industrial and Engineering Chemistry **43**(6): 1460-1467.

Engineering Data Book (2004). Hydrocarbon treating. Gas Processors Suppliers Association. Tulsa, OK. **Section 21**.

EPRI (2012). "Global CCS Institute technology series." Carbon Capture Journal: 8-9.

Feron, P. H. M. (2010). "Exploring the potential for improvement of the energy performance of coal fired power plants with post-combustion capture of carbon dioxide." International Journal of Greenhouse Gas Control **4**(2): 152-160.

Figueroa, J. D., et al. (2008). "Advancesn in CO(2) capture technology - The US Department of Energy's Carbon Sequestration Program." International Journal of Greenhouse Gas Control **2**(1): 9-20.

Frank, M. J. W., et al. (1995). "Modeling of Simultaneous Mass and Heat-Transfer with Chemical-Reaction Using the Maxwell-Stefan Theory .2. Nonisothermal Study." Chemical Engineering Science **50**(10): 1661-1671.

Frank, M. J. W., et al. (1995). "Modeling of Simultaneous Mass and Heat-Transfer with Chemical-Reaction Using the Maxwell-Stefan Theory .1. Model Development and Isothermal Study." Chemical Engineering Science **50**(10): 1645-1659.

Hailong Li, e. a. "Review of available experimental data and models for the transport properties of CO2-mixture relevant for CO2 capture, transport ans storage."

Higbie, R. (1935). "The Rate of Absorption of a Pure Gas into a Still Liquid during Short Periods Exposure." Transactions of the American Institute of Chemical Engineers **31**: 365-389.

Higbie, R. (1935). "The rate of absorption of a pure gas into a still liquid during short periods of exposure." Transactions of the American Institute of Chemical Engineers **31**: 365 - 383.

Kenig, E. Y., et al. (2001). "Reactive absorption: Optimal process design via optimal modelling." Chemical Engineering Science **56**(2): 343-350.

Kidnay, A. J., Parrish, W. R., McCartney, D. G., (2011). Fundamentals of Natural Gas Processing, Boca Raton, Fla. : CRC/Taylor & Francis.

Klinkenbijl, J. M., Dillon, M.L., Heyman, E.C., (1999). Gas pre-treatment and their impact on liquefaction processed. Proceedings of the Seventy-Eighth Annual Convention of the Gas Processors Association, Tulsa, OK.

Ko, J. J., et al. (2001). "Diffusivity of nitrous oxide in aqueous alkanolamine solutions." Journal of Chemical and Engineering Data **46**(1): 160-165.

Kohl, A. L., Nielsen, R.B., (1997). Gas Purification Houston, Gulf Publishing Company.

Krishnamurthy, R. and R. Taylor (1985). "A Nonequilibrium Stage Model of Multicomponent Separation Processes .2. Comparison with Experiment." Aiche Journal **31**(3): 456-465.

Kucka, L., et al. (2003). "On the modelling and simulation of sour gas absorption by aqueous amine solutions." Chemical Engineering Science **58**(16): 3571-3578.

Lee, J. H. and M. P. Dudukovic (1998). "A comparison of the equilibrium and nonequilibrium models for a multicomponent reactive distillation column." Computers & Chemical Engineering **23**(1): 159-172.

Littel, R. J., et al. (1992). "Kinetics of CO2 with Primary and Secondary-Amines in Aqueous-Solutions .2. Influence of Temperature on Zwitterion Formation and Deprotonation Rates." Chemical Engineering Science **47**(8): 2037-2045.

Lweis, W. K., Whiteman, W. G., (1924). "Principles of gas absorption." Industrial and Engineering Chemistry **16**: 1215 - 1220.

Mayer, J., et al. (1999). "Dynamic and steady state simulation of coke oven gas purification." Computers & Chemical Engineering **23**: S843-S846.

Murphree, E. V. (1925). "Rectifying column calculations with particular reference to N component mixtures." Industrial and Engineering Chemistry **17**(7): 747 - 750.

Ooi, S. M. P. (2008). Development and Demonstration of a New Non-Equilibrium Rate-Based Process Model for the Hot Potassium Carbonate Process. School of Chemical Engineering, The University of Adelaide. **PhD Thesis**.

Pacheco, M. A. and G. T. Rochelle (1998). "Rate-based modeling of reactive absorption of CO2 and H2S into aqueous methyldiethanolamine." Industrial & Engineering Chemistry Research **37**(10): 4107-4117.

Peng, J. J., et al. (2002). "A comparison of steady-state equilibrium and rate-based models for packed reactive distillation columns." Industrial & Engineering Chemistry Research **41**(11): 2735-2744.

Penttila, A., et al. (2011). "The Henry's law constant of N2O and CO2 in aqueous binary and ternary amine solutions (MEA, DEA, DIPA, MDEA, and AMP)." Fluid Phase Equilibria **311**: 59-66.

Peyghambarzadeh, S. M., et al. (2009). "Experimental and Theoretical Study of Pool Boiling Heat Transfer to Amine Solutions." Brazilian Journal of Chemical Engineering **26**(1): 33-43.

Ramachandran, N., et al. (2006). "Kinetics of the absorption of CO2 into mixed aqueous loaded solutions of monoethanolamine and methyldiethanolamine." Industrial & Engineering Chemistry Research **45**(8): 2608-2616.

Rao, A. B. a. R., E. S. (2002). "A Technical, Economic, and Environmental Assessment of Amine-Based CO2 Capture Technology for Power Pland Greenhouse Gas Control." Environ. Sci. Technol **36**: 9.

Rojey, A., Jafferet, C., (1997). Natural Gas Production Processing and Transport, Institut Francais Du Petrole Pbulication.

Ross, E. D. a. G., T. R. (2011). "Modeling CO2 abospriton into concentrated aqueous monoethanolamine and piperazine." Chemical Engineering Science **66**: 5212-5218.

Schneider, R. and A. Gorak (2001). "Model optimization for the dynamic simulation of reactive absorption processes." Chemical Engineering & Technology **24**(10): 979-989.

Seader, J. D. a. H., E.J. (1998). Separation Process Principles. New York, Wiley.

Sharma, M. M. and Danckwer.Pv (1970). "Chemical Methods of Measuring Interfacial Area and Mass Transfer Coefficients in 2-Fluid Systems." British Chemical Engineering **15**(4): 522-&.

Snijder, E. D., et al. (1993). "Diffusion-Coefficients of Several Aqueous Alkanolamine Solutions." Journal of Chemical and Engineering Data **38**(3): 475-480.

Taylor, R., Krishana, R. (1993). Multicomponent Mass Transfer. New York, John Wiley and Sons.

Taylor, R., et al. (2003). "Real-world modeling of distillation." Chemical Engineering Progress **99**(7): 28-39.

Udani, L. H. (1961). Mass Transfer with Chemical Reaction in View of Various Models. Department of Chemical Engineering, University of Michigan.

Vaidya, P. D. and E. Y. Kenig (2007). "CO2-Alkanolamine Reaction Kinetics: A Review of Recent Studies." Chemical Engineering & Technology **30**(11): 1467-1474.

Versteeg, G. F. and W. P. M. Vanswaaij (1988). "Solubility and Diffusivity of Acid Gases (Co2, N2o) in Aqueous Alkanolamine Solutions." Journal of Chemical and Engineering Data **33**(1): 29-34.

Weiland, R. H., et al. (1997). "Heat capacity of aqueous monoethanolamine, diethanolamine, N-methyldiethanolamine, and N-methyldiethanolamine-based blends with carbon dioxide." Journal of Chemical and Engineering Data **42**(5): 1004-1006.

Weiland, R. H., et al. (1998). "Density and viscosity of some partially carbonated aqueous alkanolamine solutions and their blends." Journal of Chemical and Engineering Data **43**(3): 378-382.

Yih, S. M., Lai, H. C. (1987). "Simultaneous absorption of carbon dioxide and hydrogen sulfide in hot carbonate solutions in a packed absorber-stripper unit." Chemical Engineering Communications **51**(1-6): 277 - 290.

Ying, J. R., et al. (2012). "Measurements and Correlation of Physical Solubility of Carbon Dioxide in (Monoethanolamine plus Water) by a Modified Technique." Industrial & Engineering Chemistry Research **51**(19): 6958-6966.

Zhicheng Xu, et al. (2013). "Kinetics Study on CO2 Absorption with Aqueous Solutions of 1,4-Butaneiamine, 2-(Diethylamino)-ethanol, and Their Mixtures." Industrial & Engineering Chemistry Research **52**: 9790-9802.

Appendix A. MATLAB Code

1. Parameter Setting

```
clear;
clc;
T=333;                                          % Temperature, [K]
P=100;                                          % Pressure, [kPa]

%-------------- CO2 initial parameter -------------------------
y_CO2=1.0;            % mole fraction of CO2 in gas bulk phase, [-]
P_CO2=P*y_CO2;        % CO2 partial pressure, [kPa]

%-------------- MEA initial parameter -------------------------
roh=1013;             % Density of aqueous MEA solutions, [kg/m3]
wt=0.3;               % Mass weight MEA, [-]
m_MEA=roh*wt*1;       % mass weight of MEA, [kg]
Mw_MEA=61.08;         % Molecular weight of MEA, [g/mol]
n_MEA=m_MEA/Mw_MEA;   % Molecular amount of MEA, [kmol]

C_MEA=n_MEA;          % MEA molecular concentration in liquid bulk phase,
C_MEA [kmol/m3]
CO2Ldg=0;             % CO2 loading, [-]
C_CO2=C_MEA*CO2Ldg;   % CO2 concentration, C_MEA [kmol/m3]
C_MEA=C_MEA-2*C_CO2; % MEA fresh concentration, [kmol/m3]

%---------- Observed reaction rate constant, k_obs [1/s] ---------
k_MEA=4.61*10^9*exp(-4421/T);
% 2nd order reaction rate constant, k_MEA [1/s]

%------- CO2 molecular diffusivity in MEA solution, D_CO2_MEA [m2/s] --
b0=5.07*10^(-6);     % b0 parameter N2O for all amine
b1=8.65*10^(-7);     % b1 parameter N2O for MEA
b2=2.78*10^(-7);     % b2 parameter N2O for MEA
b3=-2371;            % b3 paramater N2O for all amine
b4=-9.34*10;         % b4 paramter N2O for MEA
b5=2.35*10^(-6);     % b5 parameter CO2
b6=-2119;            % b6 parameter CO2

D_N2O_MEA=(b0+b1*C_MEA+b2*C_MEA^2)*exp((b3+b4*C_MEA)/T);
                    % Diffusivity of N2O in MEA solution
D_N2O_0=b0*exp(b3/T);     % Diffusivity of N2O in water
D_CO2_0=b5*exp(b6/T);     % Diffusivity of CO2 in water

D_CO2_MEA=D_N2O_MEA*D_CO2_0/D_N2O_0;
% CO2 molecular diffusivity in MEA solution, D_CO2_MEA [m2/s]

%----------------- MEA diffusivity, D_MEA [m2/s] --------------------
a=-13.275;
b=-2198.3;
c=-7.8142*10^(-5);

D_MEA=exp(a+b/T+c*C_MEA*1000);      %% MEA molecular diffusivity, [m2/s]
```

```
%-- Herny's law constant of CO2 in aquaous MEA solution, H_CO2_MEA
[kPa.m3/kmol]
%% Parameters for N2O in water
a1=158.245;
b1=-9048.596;
c1=-20.860;
d1=-0.00252;

%% Parameters for CO2 in water
a2=145.369;
b2=-8172.355;
c2=-19.303;
d2=0;

%% Parameters for N2O in pure amine (MEA)
a3=-9172.50;
b3=39.598;

H_N20_0=exp(a1+b1/T+c1*log(T)+d1*T);       % Herny's law constant of
N2O in water, [kPa.m3/kmol]
H_CO2_0=exp(a2+b2/T+c2*log(T)+d2*T);       % Herny's law constant of
CO2 in water, [kPa.m3/kmol]
H_N2O_MEA=exp((8.3194+4.52e-3*C_MEA-4.78e-2*CO2Ldg+4.56e-
2*C_MEA*CO2Ldg)-1905*(1/T-1/298.15));
% Herny's law constant of N2O in pure MEA, [kPa.m3/kmol]

H_CO2_MEA=H_N2O_MEA*H_CO2_0/H_N20_0;
% Herny's law constant of CO2 in aquarous MEA solution, [kPa.m3/kmol]

%------------------- Heat conductivity, [kW/m/K] ---------------
Mw_H2O=18;              % Molecular weight of H2O, [kg/kmol]
Mw_CO2=44;              % Molecular weight of CO2, [kg/kmol]
m_tot=roh*1;            % mass weight of solution, [kg]
n_CO2=CO2Ldg*m_MEA/Mw_MEA;     % Molecular amount of CO2, [kmol]
m_CO2=n_CO2*Mw_CO2;     % mass weight of CO2, [kg]
m_H2O=m_tot-m_MEA-m_CO2; % mass weight of H2O, [kg]
n_H2O=m_H2O/Mw_H2O;     % Molecular amount of H2O, [kmol]
n_tot=n_MEA+n_H2O+n_CO2;      % Total moles, [mol]
x_MEA=n_MEA/n_tot;      % Molar fraction of MEA, [-]
x_H2O=n_H2O/n_tot;      % Molar fraction of H2O, [-]

lambda_MEA=0.22/1000;        % Heat conductivity of MEA, [kW/m/K]
lambda_H2O=0.676/1000;       % Heat conductivity of H2O, [kW/m/K]
lambda_tot=(lambda_MEA*x_MEA+lambda_H2O*x_H2O)/10;
%% Heat conductivity of MEA solution, [kW/m/K]
```

2. Comparison of Simplified Mass Transfer Model with Project Model

```
function bvp4
xlow=0;
xhigh=0.000005;
solinit=bvpinit(linspace(xlow,xhigh,100),[0 0]);
sol=bvp4c(@bvp4ode,@bvp4bc,solinit);

xint=linspace(xlow,xhigh);
Sxint=deval(sol,xint);

%--------------------- Thesis results using bvp4c ----------------
figure;
plot(xint,Sxint(1,:),'b')
set(findobj(get(gca,'Children'),'LineWidth',0.5),'LineWidth',2);
hold on

%---------------- Project results using normal matrix ------------
X=[0,0.0000002,0.0000004,0.0000006,0.0000008,0.000001,0.0000012,0.00000
14,0.0000016,0.0000018,0.000002,0.0000022,0.0000024,0.0000026,0.0000028
];
Y=[0.0521,0.0315,0.0191,0.0115,0.007,0.0042,0.0026,0.0015,0.0009,0.0006
,0.0003,0.0002,0.0001,0.0001,0];

plot(X,Y,'d','MarkerEdgeColor','r','MarkerFaceColor','r')
hold off

set(gca,'XLim',[xlow xhigh],'xTick',[xlow:0.000001:xhigh]);
set(gca, 'Fontname', 'Times newman', 'Fontsize',
12,'FontWeight','bold');
xlabel('Distance from gas-liquid interface, z [m]')
ylabel('CO_{2} concentration in liquid film, [CO_{2}] [kmol/m^{3}]')
legend({'Thesis - Partial differential equations';'Semester Project -
Matrix equations'});

function dydx=bvp4ode(x,y)
dydx=[y(2) 6.4411e+12*y(1)];

function res=bvp4bc(ya,yb)
res=[ya(1)-0.0521 yb(1)];
```

3. Mass Transfer Model

```
function bvp4
xlow=0;
xhigh=0.000005;
solinit=bvpinit(linspace(xlow,xhigh,100),[0 0 0 0]);
sol=bvp4c(@bvp4ode,@bvp4bc,solinit);

xint=linspace(xlow,xhigh);
Sxint=deval(sol,xint);

figure;
[AX,H1,H2] = plotyy(xint,Sxint(1,:),xint,Sxint(2,:),'plot');
set(findobj(get(gca,'Children'),'LineWidth',0.5),'LineWidth',2);

set(AX(1),'xlim',[xlow,xhigh],'xTick',[xlow:0.000001:xhigh]);
set(AX(2),'xlim',[xlow,xhigh],'xTick',[xlow:0.000001:xhigh]);
set(AX(1),'XColor','k','YColor','k','FontWeight','bold');
set(AX(2),'XColor','k','YColor','k','FontWeight','bold');
HH1=get(AX(1),'Ylabel');
set(AX(1),'ylim',[0,0.06],'yTick',[0:0.01:0.06]);
set(HH1,'String','CO_{2} concentration in liquid film, [CO_{2}
[kmol/]');
set(HH1,'color','k','FontWeight','bold');
HH2=get(AX(2),'Ylabel');
set(AX(2),'ylim',[0,5],'yTick',[0:0.5:5]);
set(HH2,'String','MEA concentration in liquid film, [MEA]
[kmol/m^{3}]');
set(HH2,'color','k','FontWeight','bold');
set(H1,'color','b');
set(H2,'color','r');
legend([H1,H2],{'CO_{2} concentration, [kmol/m^{3}]';'MEA concentration,
[kmol/m^{3}]'});
xlabel('Distance from gas-liquid interface, z [m]','FontWeight','Bold');

function dydx=bvp4ode(x,y)
k_MEA=1.6622e+03;
D_CO2_MEA=1.2903e-09;
D_MEA=7.2666e-11;
dydx=[y(3) y(4) k_MEA/D_CO2_MEA*y(1)*y(2) 2*k_MEA/D_MEA*y(1)*y(2)];

function res=bvp4bc(ya,yb)
P_CO2=100;
H_CO2_MEA=3.0546e+03;
C_MEA=4.9754;
C_CO2=0;
res=[ya(1)-P_CO2/H_CO2_MEA ya(4) yb(1)-C_CO2 yb(2)-C_MEA];
```

4. Temperature Gradient

```
function bvp4
xlow=0;
xhigh=0.000005;
solinit=bvpinit(linspace(xlow,xhigh,100),[0 0 0 0]);
sol=bvp4c(@bvp4ode,@bvp4bc,solinit);

xint=linspace(xlow,xhigh);
Sxint=deval(sol,xint);

%-------------------- Reaction Heat, Q [kJ/(m^{3} s)] -----------------
figure;
Q=1.6622e+03*Sxint(1,:).*Sxint(2,:)*85;  %% Reaction Heat
plot(xint,Q,'b')
set(gca,'xlim',[xlow,xhigh],'xTick',[xlow:0.000001:xhigh]);
xlabel('Distance from gas-liquid interface, z [m]');
ylabel('Reaction Heat, Q [kJ/(m^{3} s)]');

%------------- Temperature Gradient, delta T [K/s] --------------------
Cp=3.8;                 % Specific heat capacity of MEA, [kJ/(kg(MEA) K)]
rho=1013;               % Density of MEA, [kg/m3]
deltaT=Q/Cp/rho;        % Temperature Gradient, [K/s]
figure;
plot(xint,deltaT)
set(gca,'xlim',[xlow,xhigh],'xTick',[xlow:0.000001:xhigh]);
xlabel('Distance from gas-liquid interface, z [m]');
ylabel('Temperature Gradient, delta T [K/s]');

function dydx=bvp4ode(x,y)
dydx=[y(3) y(4) k_MEA/D_CO2_MEA*y(1)*y(2) 2*k_MEA/D_MEA *y(1)*y(2)];

function res=bvp4bc(ya,yb)
res=[ya(1)- P_CO2/H_CO2_MEA ya(4) yb(2)-5 yb(3)];
```

5. Heat Transfer Model

```
function bvp4
xlow=0;
xhigh=0.000005;
solinit=bvpinit(linspace(xlow,xhigh,100),[0 0 0 0 0 0]);
sol=bvp4c(@bvp4ode,@bvp4bc,solinit);

xint=linspace(xlow,xhigh);
Sxint=deval(sol,xint);

%--------------- Temperature Profile in liquid film, T [K] ------------
plot(xint,Sxint(3,:))
set(gca,'xlim',[xlow,xhigh],'xTick',[xlow:0.000001:xhigh]);
% set(gca,'ylim',[298,298.16],'yTick',[298:0.04:298.16]);
xlabel('Distance from gas-liquid interface, z [m]');
ylabel('Temperature, T [K]');

function dydx=bvp4ode(x,y)
dydx=[y(4) y(5) y(6) k_MEA/D_CO2_MEA*y(1)*y(2) 2*k_MEA/D_MEA*y(1)*y(2)
1/lambda_tot*k_MEA*[MEA]*[CO2]*h_CO2+2*k_MEA*[MEA]*[CO2]*h_MEA];

function res=bvp4bc(ya,yb)
res=[ya(1)- P_CO2/H_CO2_MEA ya(5) ya(6) yb(2)-5 yb(4) yb(3)-298];
```

Appendix B. Absorption Equilibrium Film Thickness

1. Effects of operation temperature

Operation temperature, [K]	Thickness, [*10^{-6}m]
298	3
313	2.5
333	2

2. Effects of CO_2 loading

CO_2 loading, [mol/mol]	Thickness, [*10^{-6}m]
0	2.5
0.2	3
0.4	6

3. Effects of MEA mass weight

MEA mass weight, [wt%]	Thickness, [*10^{-6}m]
10 wt%	4.4
20 wt%	3
30 wt%	2.3

Appendix C. Temperature Rise at Interface

1. Effects of operation temperature

Operation temperature, [K]	Temperature rise at interface, [K]
298	0.077
313	0.142
333	0.146

2. Effects of CO2 loading

CO_2 loading, [mol/mol]	Temperature rise at interface, [K]
0	0.074
0.2	0.056
0.4	0.028

3. Effects of MEA mass weight

MEA mass weight, [wt%]	Temperature rise at interface, [K]
10 wt%	0.04
20 wt%	0.062
30 wt%	0.075

4. Matrix analysis

CO_2 loading, [mol/mol]	Operation Temperature, [K]	Temperature rise at interface, [K]
0	298	0.077
	313	0.102
	333	0.146
0.2	298	0.056
	313	0.086
	333	0.119
0.4	298	0.028
	313	0.048
	333	0.068

CO_2 loading, [mol/mol]	MEA mass weight, [wt%]	Temperature rise at interface, [K]
0	10 wt%	0.04
	20 wt%	0.061
	30 wt%	0.074
0.2	10 wt%	0.029
	20 wt%	0.048
	30 wt%	0.056
0.4	10 wt%	0.014
	20 wt%	0.025
	30 wt%	0.028

Operation Temperature, [K]	CO_2 loading, [mol/mol]	Temperature rise at interface, [K]
298	0	0.074
	0.2	0.056
	0.4	0.028
313	0	0.103
	0.2	0.086
	0.4	0.048
333	0	0.146
	0.2	0.119
	0.4	0.068

Operation Temperature, [K]	MEA mass weight, [wt%]	Temperature rise at interface, [K]
298	10 wt%	0.04
	20 wt%	0.061
	30 wt%	0.074
313	10 wt%	0.055
	20 wt%	0.083
	30 wt%	0.103

Operation Temperature, [K]	MEA mass weight, [wt%]	Temperature rise at interface, [K]
333	10 wt%	0.078
	20 wt%	0.118
	30 wt%	0.146

MEA mass weight, [wt%]	Operation Temperature, [K]	Temperature rise at interface, [K]
10 wt%	298	0.04
	313	0.055
	313	0.078
20 wt%	298	0.061
	313	0.083
	313	0.118
30 wt%	298	0.074
	313	0.103
	313	0.146

MEA mass weight, [wt%]	CO_2 loading, [mol/mol]	Temperature rise at interface, [K]
10 wt%	0	0.04
	0.2	0.029
	0.4	0.014
20 wt%	0	0.061
	0.2	0.048
	0.4	0.025
30 wt%	0	0.074
	0.2	0.056
	0.4	0.028